nature reviews earth & environment

https://doi.org/10.1038/s43017-024-00531-3

Review article

Check for updates

The role of biota in the Southern Ocean carbon cycle

Philip W. Boyd [1,2,3] ✉, Kevin R. Arrigo [4], Mathieu Ardyna [5], Svenja Halfter [6], Luis Huckstadt [7], Angela M. Kuhn [8], Delphine Lannuzel [1,2,3], Griet Neukermans [9,10], Camilla Novaglio [3], Elizabeth H. Shadwick [2,11], Sebastiaan Swart [12,13] & Sandy J. Thomalla [14,15]

Abstract

The Southern Ocean, although relatively understudied owing to its harsh environment and geographical isolation, has been shown to contribute substantially to processes that drive the global carbon cycle. For example, phytoplankton photosynthesis transforms carbon dioxide into new particles and dissolved organic carbon. The magnitude of these transformations depends on the unique oceanographic and biogeochemical properties of the Southern Ocean. In this Review, we synthesize observations of biologically mediated carbon flows derived from the expanded observational network provided by remote-sensing and autonomous platforms. These observations reveal patterns in the magnitude of net primary production, including under-ice blooms and subsurface chlorophyll maxima. Basin-scale annual estimates of the planktonic contribution to the Southern Ocean carbon cycle can also be calculated, indicating that the export of biogenic particles and dissolved organic carbon to depth accounts for 20–30% (around 3 Gt yr^{-1}) of the global export flux. This flux partially compensates for carbon dioxide outgassing following upwelling, making the Southern Ocean a 0.4–0.7 Gt C yr^{-1} sink. This export flux is surprisingly large given that phytoplankton are iron-limited with low productivity in more than 80% of the Southern Ocean. Solving such enigmas will require the development of four-dimensional regional observatories and the use of data-assimilation and machine-learning techniques to integrate datasets.

Sections

A full list of affiliations appears at the end of the paper. ✉e-mail: philip.boyd@utas.edu.au

Key points

- Increasing coverage from a suite of observations from autonomous platforms will reduce uncertainties on estimates of key processes in the regional carbon cycle that determine the magnitude of the Southern Ocean carbon sink.
- Episodic storms enhance chlorophyll stocks, presumably owing to enhanced iron supply from depth, but also drive concurrent carbon dioxide outgassing, with unknown cumulative effects on the regional carbon cycle.
- The influence of climate change on the Southern Ocean and Antarctica is expected to alter the partitioning of basin-scale net primary production between open water, sea ice and under ice.
- Observations from profiling robotic floats are providing important insights into how the fate of phytoplankton carbon drives regional patterns in export flux in the ocean's interior over multiple annual cycles.
- The inability to remotely measure dissolved iron or dissolved organic carbon concentrations makes it difficult to understand pivotal processes in the Southern Ocean carbon cycle.
- Models using data assimilation are already providing promising guidelines on how to deploy autonomous platforms to address key questions around the regional carbon cycle.

Introduction

The Southern Ocean (SO) is the key global connector of ocean basins[1]. It surrounds Antarctica and features circumpolar boundaries such as the Polar Front, which separates the sub-Antarctic 'ring' from polar waters to the south. The main circulation feature driving SO dynamics is the Antarctic Circumpolar Current, which modulates the meridional overturning circulation. This modulation leads to the formation of a biogeochemical divide in the upper ocean, whereby lower meridional overturning circulation cells control air–sea carbon dioxide (CO_2) exchange and the upper cells control global export production. However, the geographical isolation and harsh environment make the SO difficult to research. Despite being understudied, the SO is known to make a critical contribution to the Earth's carbon cycle[2,3]. Additionally, simulations suggest that the biological carbon pump (BCP) in the SO contributes disproportionately more to the global carbon sink than in other regions[4–6].

The SO transports carbon between ocean basins[7]. For example, southward-flowing deep waters upwell to the surface along steeply sloped isopycnals (density contours) in the Antarctic Circumpolar Current and transform into intermediate and mode waters, which feed the upper cell of the meridional overturning circulation, or into bottom waters that drive the lower cell, which forms Antarctic Bottom Water[1]. These cells have fundamentally different mechanisms by which they transport waters with high concentrations of CO_2 and nutrients formed by the respiration of particulate organic carbon (POC) at depth in other basins. The upper cell releases CO_2 into the atmosphere, whereas the lower cell returns these waters to great depth[2,8,9]. These physical oceanographic mechanisms are thought to be the primary drivers that make the SO a sink (0.79 ± 0.13 Gt C yr^{-1}, from multi-models[3]) for anthropogenic CO_2 (refs. 3,8–10). However, the relative contribution of the SO BCP to the regional and global carbon cycle is poorly understood, hindered by a lack of observations.

Nevertheless, biogeochemical observations — as grouped into three general eras (Fig. 1) — have led to a substantial change in the understanding of the SO. Era 1 began in the 1920s, was centred on ship-based exploration and was limited to a few months each year. These expeditions could vertically profile the ocean at coarse resolution (tens of kilometres) and revealed the fundamental characteristics of the SO, including strong westerly winds, and seasonal sea-ice formation and decline. Additionally, large populations of fish, birds and marine mammals were observed in the waters surrounding Antarctica, despite apparently low rates of net primary production (NPP)[11–14]. Era 2 was characterized by satellite observations from 1978 onwards that complemented data from ongoing research voyages. For example, satellite ocean-colour instruments observed the spatial distribution of phytoplankton abundance in surface waters (the upper few metres) over much of the SO throughout the entire year. These observations enabled the first pan-Antarctic scale estimates of the net rate of photosynthetic carbon fixation by phytoplankton after correcting for respiration (that is, through the calculation of NPP) in the SO[15–17], revealing that early ship-based estimates were 2–3-fold too low. However, these satellite measurements can provide details only of the ocean surface.

Era 3, which began in 2014 (refs. 18,19), involved technological advances associated with autonomous platforms for ocean observations that have enabled more subsurface measurements to robustly assess the magnitude of processes in the ocean interior, such as the BCP in the SO[3]. Some nations have initiated regional observing systems such as Southern Ocean Carbon and Climate Observations and Modeling project (SOCCOM) by the USA and Southern Ocean and CLIMate (SOCLIM) by France, and these have stimulated participation by other countries. Thousands of miniaturized, automated and remotely operated sensors have been deployed on gliders, uncrewed surface vehicles, bio-logging marine mammals, and robotic profiling floats, thus improving observational coverage of the surface and subsurface ocean. These sensor constellations can obtain vertical profiles of temperature, salinity, pH, dissolved oxygen, light, fluorescence (a proxy for chlorophyll stocks), particle backscatter (a proxy for POC concentrations) and nitrate concentration. These technologies have revealed important information about ocean processes ranging from winter CO_2 outgassing[20,21], hydrothermal iron plumes[22], subsurface chlorophyll maxima[23], subsurface particle export pulses and their seasonality[24], to potential under-ice blooms[25–27]. This information fills knowledge gaps about the regional carbon cycle[3] and biogeochemical functioning[7] of the SO identified by models.

In this Review, we explore the many roles of biota and plankton in the SO carbon cycle. We use additional data from the observational technologies that have been developed throughout era 3 (the autonomous era) to reassess patterns of basin-scale carbon biogeochemistry and the subsequent fate of carbon. We then explore how resident biota, along with ocean circulation, influence the SO carbon cycle. Finally, we discuss how the increasing suite of data in space (three dimensions) can be best integrated into a four-dimensional (4D) temporal observatory to detect and attribute the myriad biogeochemical roles of SO biota.

Environmental controls on phytoplankton productivity

To understand primary productivity patterns in the SO, it is important to link them with the underlying physico-chemical properties

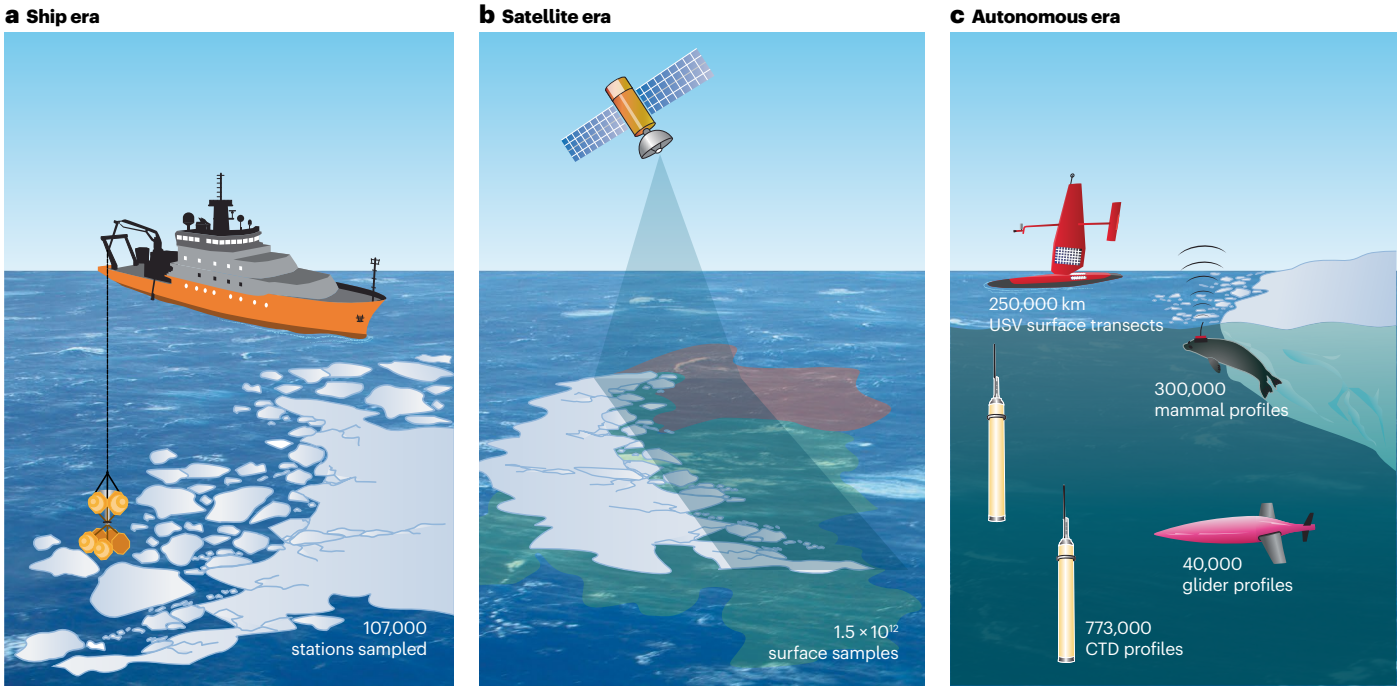

Fig. 1 | The three eras of oceanographic investigation. a, The ship era of Southern Ocean investigation (1920s–1977), providing an estimated 107,000 data points (based on 5.7 voyages annually with 150 stations per voyage since 1900). **b**, The satellite era (1978 to present), providing 1.5×10^{12} surface samples (based on four satellites collecting daily data with 4-km resolution). **c**, The autonomous era (2014 to present), providing measurements of 773,000 conductivity temperature and depth (CTD) profiles using Argo profiling floats, 42,709 chlorophyll profiles from biogeochemical Argo (BGC-Argo) floats, 40,000 glider profiles, 250,000 km of surface ocean transects by uncrewed surface vehicles (USVs), and 300,000 profiles from marine mammals (based on a tag operating for 200 days and providing three tags daily; Mark Hindell, personal communication). Together, the three eras provide a potent combination of mechanistic understanding and validation (ships), broad regional and temporal coverage (satellites) and water-column coverage (autonomous platforms).

that determine the NPP and influence the carbon cycle. For example, the wide range of iron supply mechanisms result in diverse patterns of NPP and phytoplankton stocks, as discussed here.

The high-nutrient low-chlorophyll puzzle

The SO has low chlorophyll stocks despite having perennially high nutrient concentrations, which is known as the high-nutrient low-chlorophyll (HNLC) puzzle. Understanding of this puzzle has evolved throughout the three eras of observations. HNLC waters were first identified by shipboard observations in era 1. In era 2, satellites revealed regions that departed from the HNLC trend, such as: high-chlorophyll polynyas in the marginal ice zone and seasonal ice zone; blooms downstream of both shallow bathymetry and islands; interannual variability in sea-ice extent; and differences in the seasonal cycle (phenology) of NPP across the SO[28,29]. Autonomous observations in era 3 have provided additional biogeochemical details about the HNLC ocean, including hydrothermally stimulated phytoplankton blooms[22] and the role of storms in driving variability patterns in chlorophyll stocks[30] and NPP[31,32].

Various environmental factors have been invoked to explain the HNLC puzzle, including iron limitation[33], light[34] and grazing[35]. Subsequent laboratory[36] and mesoscale field[37] experiments have confirmed that iron limitation is widespread across the SO. Additionally, the occurrence of dissolved iron hotspots such as in frontal regions[38] led to high-chlorophyll waters. Therefore, iron supply heavily influences SO carbon biogeochemistry because it determines the magnitude of NPP and influences its fate (for example, direct export of phytoplankton blooms). Furthermore, there are various iron supply mechanisms in the SO[39], some of which are linked to oceanic, atmospheric, sedimentary, hydrothermal or cryospheric processes. Iron primarily comes from the upwelling and seasonal entrainment of deeper iron-enriched waters[39,40]. However, other supply mechanisms, including the input of dust to the SO[41,42], local dust events downstream of ice-free land masses[43–45], aerosols from wildfires[46,47], and volcanic activity on islands[48] can also influence the spatial and temporal extent (Fig. 2) of iron-enhanced NPP. Additionally, meltwater from sea ice, drifting icebergs and ice shelves can potentially fertilize Antarctic surface waters with iron[49–53]; however, in situ measurements of these mechanisms are rare.

Modes of iron supply

Iron supply is driven on four timescales: episodic, for example, storms[54,55], fine-scale eddies and deposition of dust[42] or wildfire aerosols[46,47]; seasonal, including sea-ice retreat[56,57] and iceberg calving, drift and melt[58,59]; synoptic, such as pelagic iron recycling[60–63], and upwelling[40]; and sustained, including sediment resuspension[30] and hydrothermal supply[39,40] (Fig. 2). These modes influence spatiotemporal NPP patterns across the entire SO basin. For example, ships and satellites have observed high chlorophyll concentrations in island wakes[63] or blooms stimulated by wildfire-derived aerosols[46]. Additionally, robotic profiling floats observed a massive hydrothermally

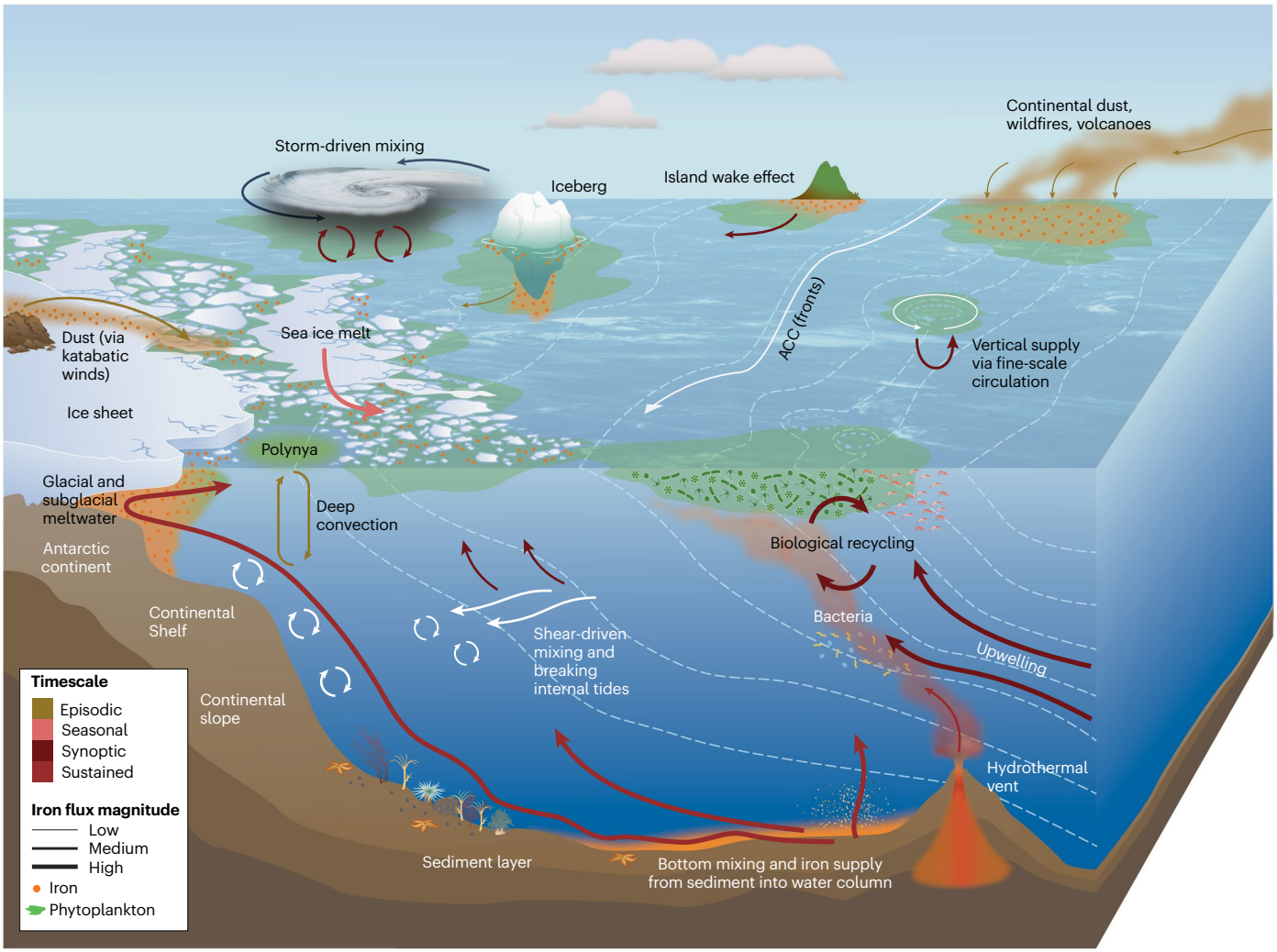

Fig. 2 | Processes and timescale of iron supply in the Southern Ocean. Physical and biological processes drive iron supply to the euphotic zone on episodic (dark yellow), synoptic (dark red), seasonal (pink) and sustained (red) timescales. Iron supply is also driven by ocean circulation (dashed and solid white arrows) including the Antarctic Circumpolar Current (ACC, solid white arrows). The magnitude of the dissolved iron (DFe) flux is represented by the thickness of the arrow, with thin, medium and thick arrows for low (<0.001 µmol DFe m^{-2} day^{-1}), medium (0.001–0.1 µmol DFe m^{-2} day^{-1}) and high (>0.1 µmol DFe m^{-2} day^{-1}) fluxes, respectively, based on refs. 38,40,42,44,57,61,70,233–242. The wide range of different iron supply mechanisms results in a complex pattern of phytoplankton productivity.

supplied iron-mediated phytoplankton bloom[22] and glider-based measurements identified a bloom during a wind-driven sustained upwelling event[64].

Iron supply determines the magnitude of chlorophyll stocks and NPP, and hence patterns within biogeochemical provinces in various ways. In polar waters, upwelling of iron drives a positive relationship between the Southern Annular Mode — the dominant mode of atmospheric variability that influences the westerly wind belt in the SO — and satellite-derived chlorophyll[65]. Similarly, overlaying phytoplankton bloom events on maps of iron supply suggests that iron availability influences NPP[66]. However, in other cases phytoplankton iron requirements have appeared to remain constant from year to year across the SO, suggesting that iron supply could have little influence upon satellite-derived chlorophyll stocks[67] or that the cumulative iron supply in the SO is constant. Satellite chlorophyll time-series decomposition suggests that episodic short-term events (such as storms) drive small-scale fluctuations in chlorophyll concentrations throughout the year[30]. Thus, the relationship between the variability of the iron supply mechanisms and carbon biogeochemistry appears to be driven across a range of spatial scales from large[28,64] to small[30].

SO primary productivity

NPP underpins the productivity of the SO, including its foodwebs and the regional carbon cycle. Therefore, to interpret spatial and temporal patterns in the magnitude of NPP it is necessary to understand regional and temporal variations in environmental controls on productivity — such as iron, light and silicate concentration (Fig. 3). The influence of these controls on NPP in oceanic, sea-ice and under-ice regions is discussed here, as is their role in determining phytoplankton community structure.

Pelagic NPP

Satellite-based estimates reveal variations in annual NPP across the SO (Fig. 3a); it is likely that these trends are linked to environmental forcing. Rates of spatially integrated NPP for the entire SO (all waters south of 50° S) are in the range 2.0–2.6 Gt C yr^{-1} (refs. 15,17,68). The lowest rates are generally associated with pelagic waters north of the seasonal ice zone, where strong westerly winds and convective mixing leads to deep mixed layers and hence phytoplankton encounter low mean light levels[34]. Consequently, the surface ocean must stratify, either through ice melt or solar heating, before a phytoplankton bloom can occur. Additionally, these waters are often deficient in trace elements such as iron[36,69–74], manganese[75–78], and vitamin B-12 (ref. 79). Incomplete macronutrient utilization owing to trace-metal limitation results in the outgassing of 0.4 Gt C yr^{-1} of natural CO_2 south of 44° S (ref. 80).

Most NPP in the SO occurs within the surface mixed layer in spring, when there is sufficient light and iron available to support phytoplankton growth. Additionally, shipboard measurements indicate that oceanographic fronts such as the Antarctic Polar Front can double the NPP of pelagic waters owing to the divergence of surface waters, which brings nutrients and dissolved inorganic carbon to the surface[17]. A similar increase in the NPP also occurs downstream of shallow topography (for example, the Scotia Sea and Kerguelen Plateau), where the interaction of currents with the seafloor increases the flux of trace metals into surface waters[79]. However, the highest rates of NPP in the SO are generally found on continental shelves and their associated coastal polynyas (Fig. 3b) where reduced ice cover and glacial meltwater-induced upwelling can increase NPP to over 2 g C m^{-2} day^{-1} (refs. 81–83) (compared with around 0.6 g C m^{-2} day^{-1} in HNLC iron-limited waters[15,16]).

In other SO basins, such as the Indian Ocean, additional NPP can occur at depth within the subsurface chlorophyll maximum — a specialized niche for some phytoplankton groups. However, such regions are relatively sparse in the SO, with ship sampling revealing few areas with a persistent or recurring subsurface chlorophyll maximum[84]. Such maxima form through various processes, including sinking[85] or subduction[86] of surface blooms, photoacclimation to low light at deeper depths[87], and increased growth rates at the nutricline when light is still causing net growth[88]. These features are too deep to be observed with satellite sensors, so subsurface chlorophyll maxima have been largely undetected. However, during era 3 the prevalence of these features could become better understood as gliders and floats provide more data on vertical phytoplankton distributions, which can be combined with satellite data to produce a more accurate three-dimensional representation of phytoplankton biomass.

Sea-ice NPP

Large-scale estimates of NPP in Antarctic sea ice are scarce but suggest that rates could vary from 23–70 Tg C yr^{-1} (that is, 0.02–0.07 Gt C yr^{-1}) (refs. 15,89,90), which equates to about 10–25% of the total water column NPP (Fig. 3c). Antarctic sea ice has a diverse phytoplankton community dominated by diatoms (mostly pennates) but also includes dinoflagellates and haptophytes[91–93]. The largest biomass often resides in the bottom sea ice where nutrients are plentiful and light is sufficient for net growth in the spring[94,95].

Substantial rates of NPP also take place within the seasonal ice zone at the interface of the ocean and the cryosphere (Fig. 3c) and represents an important resource for zooplankton in early spring, when no other food sources are available[93]. Changes in sea-ice extent, along with snow and ice thickness, alter the amount of light incident on surface waters but also modulate the amount of habitat available for resident sea-ice primary producers. For most of the satellite record, the amount of sea ice formed each year has increased owing to a persistently positive Southern Annular Mode[96,97], despite CMIP6 (Coupled Model Intercomparison Project phase 6) results predicting a decline over the same period[98]. However, in 2016, the maximum sea-ice extent in winter decreased by 2 million km^2 owing to a combination of weak winds and warmer ocean temperatures caused by El Niño[98]. Since then, data from the National Snow and Ice Data Centre show that the summertime minimum extent record was surpassed in

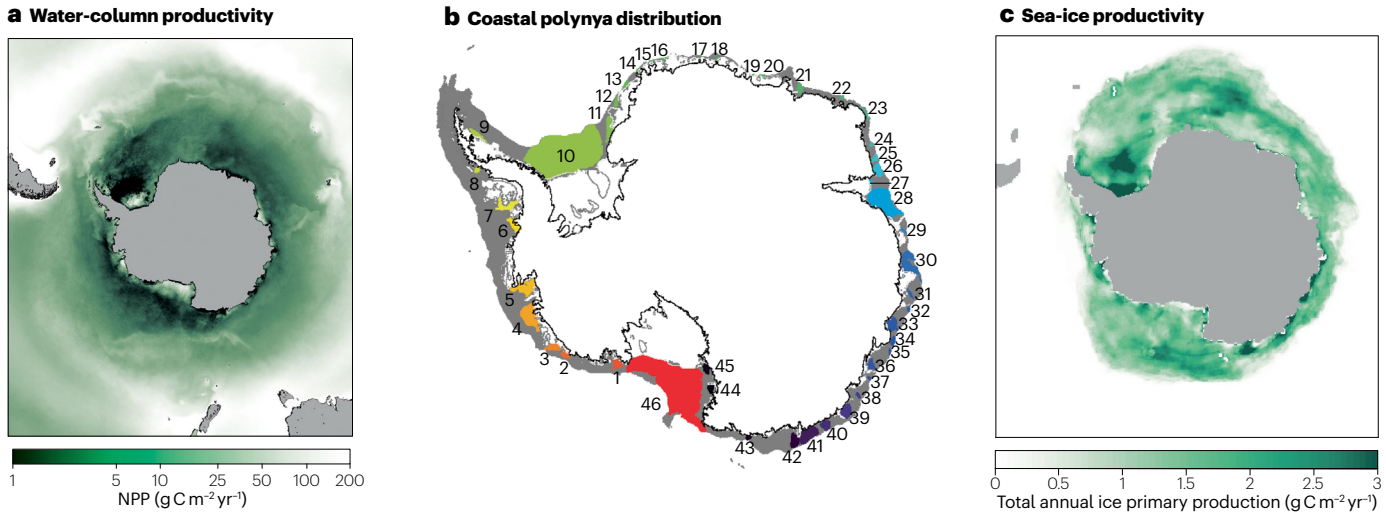

Fig. 3 | Distribution of annual net primary production in the Southern Ocean. a, Net primary production (NPP) in the water column based on satellite observations. **b**, 46 coastal polynyas, which serve as productivity hotspots along the Antarctic margin, identified using passive microwave data from satellites. **c**, Annual productivity in sea ice calculated using a data-bounded Sea Ice Ecosystem State model from ref. 90. Productivity within the sea ice is much less than that in the water column or in coastal polynyas. Part **a** is adapted from ref. 243, CC BY 3.0 https://creativecommons.org/licenses/by/3.0/). Part **b** is adapted with permission from ref. 81, AGU.

2017, 2022 and 2023. It is not known how this altered sea-ice retreat will influence sea-ice NPP or carbon biogeochemistry. Additionally, there is no record of whether Antarctic sea ice has thinned since satellite records began.

Under-ice NPP

Since 2012, large well developed phytoplankton blooms have been observed deep within the ice pack[99,100] in the Arctic Ocean as well as in the seasonal ice zone. In contrast, ship-based platforms have yet to observe such blooms in the SO; however, data from biogeochemical Argo (BGC-Argo) floats suggest that under-ice phytoplankton blooms might be present[25,26,101]. Such floats reported early bloom development and high phytoplankton biomass below sea ice, with a maximum chlorophyll-*a* value of 0.1–3.5 mg m^{-3} (refs. 25–27,101). Sea-ice dynamics, notably the snow load and associated freeboard (that is, the thickness of sea ice protruding above the ocean), control the growth of phytoplankton below the ice by modulating how much light they receive[25]. Float-based observations found that 26% of the floats beneath the ice measured chlorophyll-*a* values greater than 1.13 mg m^{-3} and the accompanying CMIP6 Earth system modelling (in which the land, ocean, atmosphere and cryosphere are fully coupled) found that 3–5 million km^2 of the ice-covered SO had sufficient light to support under-ice blooms[26]. These findings suggest that this zone is an important source of NPP that has not yet been quantified using standard ship- and satellite-based methods and that should be investigated with floats and gliders.

Phytoplankton community composition

In addition to rates of NPP, community composition can have a pronounced influence on SO carbon biogeochemistry. Shipboard and satellite observations indicate that SO phytoplankton blooms contain various species but are dominated by two broad taxa: diatoms and haptophytes (coccolithophores and prymnesiophytes). Coccolithophores often dominate at mid-SO latitudes and during the austral summer and early autumn they form a circumpolar ring of water with high $CaCO_3$ concentration known as the Great Calcite Belt[102] (GCB), which has been observed using satellite-based[102] and in situ[102,103] measurements. The GCB accounts for around 25% of the abundance of coccolithophores worldwide[104] and regulates the surface water alkalinity and the rate of air–sea CO_2 exchange. Dissolution of $CaCO_3$ in deep water (which consumes CO_2 and reduces supersaturation) also limits CO_2 outgassing from upwelled waters[105].

Further south, phytoplankton blooms are dominated by diatoms (such as *Chaetoceros, Coscinodiscus, Nitzschia, Fragilariopsis* and *Thalassiosira*) or the colonial prymnesiophyte *Phaeocystis antarctica*. It is likely that diatom blooms, which are more readily grazed but more efficient exporters of organic carbon than *P. antarctica*, are the most widespread taxa in this region[106]. However, blooms dominated by *P. antarctica*, which take up twice the amount of CO_2 per unit phosphate consumed compared to diatoms, have been observed in the Ross Sea[83,106,107], the Amundsen Sea[108–110], offshore over the Australian–Antarctic Ridge[111], the Weddell Sea[112–114] and along the western Antarctic Peninsula in spring (diatoms dominate there in summer)[115]. Whether diatoms or *P. antarctica* dominate in a region seems to be determined by light and iron availability[106,116,117] and perhaps sensitivity to ocean pH[118]. Cryptophyte blooms have been observed occasionally in the SO, but these are usually restricted to nearshore waters with substantial glacial melt[107,119]. Hence, floristics and NPP have a joint role in driving key carbon cycle processes, such as export flux, of the SO.

Temporal trends in NPP

Although NPP can be calculated from data collected by profiling floats, the coverage will be far less than that provided by satellite remote sensing. Additionally, there are fewer years of float-based measurements than for satellite records and floats have not resampled the same areas frequently enough to say much about interannual variability. Therefore, the best option for making large-scale estimates of NPP could be to combine the vertical distributions of phytoplankton obtained from float data with the horizontal distributions of phytoplankton provided by satellite data.

Satellite records show that the interannual variability in NPP across the SO is low compared to other oceans[15,30], especially the Arctic Ocean where NPP varied by 57% during 1998–2018 (ref. 120). The low interannual variability of NPP in the SO is partially attributed to the small interannual differences in sea-ice cover for most of the satellite record (until the large decline beginning in 2016)[98]. During this time there was low interannual variability in the NPP of offshore waters[15] as well as on the continental shelf in coastal polynyas[81], with regional increases in one area often balancing regional losses in others. Interannual variability in the SO appears to be driven by sub-seasonal variation due to intermittent small-scale forcing[30]. For example, shifting wind patterns and sea-ice distributions[121] in the highly productive Ross, Bellingshausen, and Amundsen seas[122] that are associated with different phases of the Southern Annular Mode are partly responsible for introducing variability in NPP.

Chlorophyll is more interannually and regionally variable than pan-Antarctic NPP[123,124]. This increased variability is expected because variation in daily NPP is correlated to the square root of surface chlorophyll concentration[125]. Other parameters related to NPP can also be more interannually variable than NPP. For example, changes in the timing (phenology) and magnitude of phytoplankton bloom depend on sub-seasonal variability in atmospheric[126] and sea-ice processes[127,128] and large-scale climate patterns such as the Southern Annular Mode[129,130].

Most models project that climate change is likely to increase the productivity of the SO through a loss of sea ice and a temperature-mediated increase in phytoplankton growth rates[131–133]. Additionally, the magnitude of future NPP could also be influenced by changes in nutrient biogeochemistry[134], a transition from a deeper mixed layer to stronger stratification[135], altered phenology[136], and possible shifts toward smaller-sized phytoplankton[116,137,138]; however, the specific effects of these variables remains unknown. Increases in NPP will have implications not only for the SO carbon cycle but also for the global carbon cycle because an increased demand for nutrients in the SO will reduce the lateral supply northward[10,139]. Many of the processes that determine the direction, magnitude and rates of change of SO biogeochemistry are not well understood; therefore, current models (such as CMIP6) do not agree on the direction of predicted changes in the productivity and CO_2 fluxes in the SO[140,141].

Fate of phytoplankton stocks

Spatial and temporal variability in NPP drives corresponding increases in phytoplankton stocks, which have a wide range of fates within the SO carbon cycle, the simplest of which is direct sinking of phytoplankton to depth. Alternatively, grazing can re-route carbon by increasing the biomass of pelagic higher trophic levels, or by transporting or releasing waste products such as dissolved organic carbon (DOC) at depth. Here, these carbon transformations are explored as the first step to elucidating the influence of biologically modulated controls on the SO carbon cycle.

Herbivory

Grazing of phytoplankton, termed herbivory, is the starting point of the transfer of carbon through foodwebs to higher trophic levels (apex predators). Herbivory and subsequent transfers can also move carbon to other pathways within the SO carbon cycle (for example, faecal pellets in the BCP). Profiling float data suggest that herbivory accounts for 90% of the annual NPP in the seasonal ice zone[142], confirming that herbivory can have a major influence on NPP in the SO. However, there are large uncertainties associated with modelled estimates of grazing owing to the various formulations by which grazing can be described[143].

Observational datasets[144] combining summer satellite measurements of ocean colour and ship-based observations such as KRILLBASE, which provides information on Antarctic krill (*Euphausia superba*) and salps (family Salpidae)[145] are used to calculate how much carbon is transferred to zooplankton biomass during herbivory. These datasets reveal an inverted biomass pyramid (Fig. 4a,b) with biomass increasing by up to 1.5 times from phytoplankton to mesozooplankton (Supplementary Fig. 1). Mesozooplankton (67 Mt) accounts for two times more biomass than krill and over 60 times more than salps. This inversion is most conspicuous at mid-latitudes of 50–70° S, whereas biomass in the Pacific sector and the highest latitudes is dominated by phytoplankton. Despite the many assumptions linked to such compound observational datasets[144], several mechanisms have been proposed to explain this inverted biomass pyramid. The most compelling mechanism, which is supported by biomass observations of mesozooplankton (such as copepods), krill and phytoplankton, is that predators have a substantially larger biomass than that of their phytoplankton prey. These high predator:prey mass ratios (>4,000; ref. 146) could compensate for the effects of low trophic transfer efficiency (often about 10%).

Transfer to higher trophic levels

Owing to a paucity of observations, it is challenging to link the transfer of carbon biomass to trophic levels higher than krill. However, advances are being made by combining and comparing phytoplankton and zooplankton simulations from Earth system models as well as higher trophic level simulations from marine ecosystem models. Here, we consider marine ecosystem models that contribute to the Fisheries and Marine Ecosystem Model Inter-comparison Project[147] (FishMIP) and Earth system models that provide phytoplankton and zooplankton inputs for such marine ecosystem models.

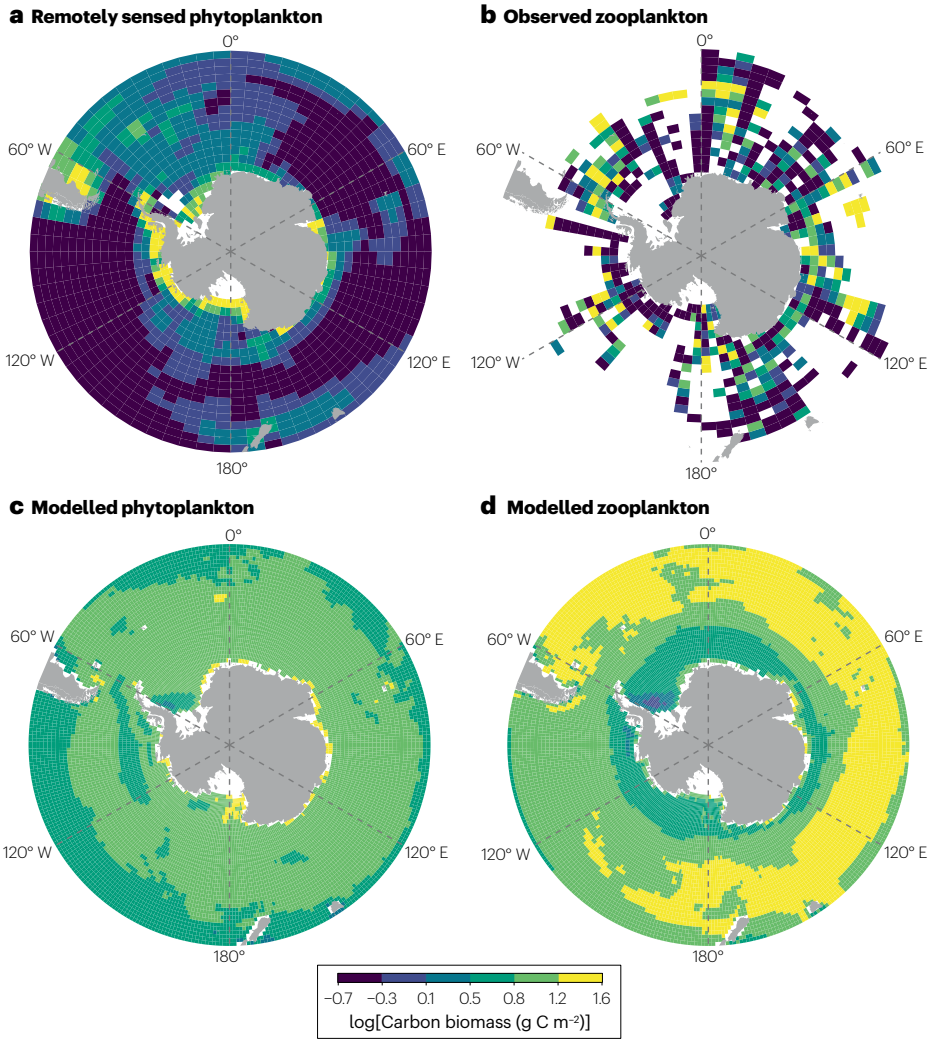

Fig. 4 | The transfer of Southern Ocean productivity to grazers. a, Depth-integrated (surface layer) phytoplankton carbon biomass for the austral summer months (December to March) based on the multiyear (1998–2020) mean summer chlorophyll measurements from satellite observations of ocean colour (ESA OC-CCI). **b**, As in **a**, but for mesozooplankton, based on stock data from ref. 144 and KRILLBASE[145]. White regions indicate areas for which there is no data available. **c**, Modelled depth integrated (water column) phytoplankton carbon biomass for the austral summer months (December to March) and averaged across 1995–2014 and two Earth system models, IPSL-CM6A-LR and GFDL-ESM4 (ref. 244). **d**, As in **c**, but for zooplankton. The range of values is kept between 0.5 and 5 g C m^{-2}, in logarithmic scale, to allow better comparison between panels and to highlight geographical patterns. These comparisons reveal the relationship between predator and prey biomass that in turn sets patterns in the stocks of higher trophic levels (Supplementary Figs. 1–4). Parts **a** and **b** are adapted from ref. 144, CC BY 3.0 https://creativecommons.org/licenses/by/3.0/.

Satellite-derived and empirical estimates of phytoplankton and zooplankton carbon for the austral summer months[144] (0.3–8.4 g C m^{-2} and 0–24 g C m^{-2}, respectively) have a wider range than estimates obtained from Earth system model simulations (1.3–5.7 g C m^{-2} for phytoplankton, and 0.9–5.5 g C m^{-2} for zooplankton, Supplementary Fig. 2). These differences could be caused by sampling biases and modelling assumptions, or discrepancies in the type and spatio-temporal coverage of the satellite and empirical data relative to that of the modelled data. However, observations and simulations both show that in the majority of grid cells the biomass of zooplankton is larger than that of phytoplankton (Fig. 4 and Supplementary Figs. 1 and 2). Although less enhanced, this pattern is also evident when considering whole-year, instead of summer, modelled plankton biomass. Large empirical estimates of zooplankton biomass are scattered around Antarctica and mostly occur in the Indian Ocean and off eastern South America. Similarly, in model simulations high zooplankton stocks are found in the Indian and South Atlantic Ocean and in particular along the east coast of South America.

FishMIP marine ecosystem models use phytoplankton and/or zooplankton biomasses obtained with Earth system models to produce simulations of size-resolved consumer biomass to represent higher trophic levels. The modelled consumer biomass decreases as the body size of the marine organisms increases, which is consistent with a bottom-heavy trophic structure (Supplementary Fig. 3). This trend is opposite to that observed between phytoplankton and zooplankton (Fig. 4 and Supplementary Fig. 2). Specifically, the biomass of the smallest size class (1–10 g) is in the range 1.7–7.1 g C m^{-2} across grid cells, whereas the biomass of the largest size class (10–100 kg) is in the range 0.6–2.8 g C m^{-2}. Maps of the simulated consumer biomass and of biomass ratios across size classes confirm the consistent decrease in biomass with increasing body size for biomasses of 0.5–5 g C m^{-2} (Supplementary Figs. 3 and 4).

However, model simulations also provide some evidence for biomass inversions in higher trophic levels (Supplementary Fig. 4). For example, simulated biomass ratios between the 1–10 g class and lower trophic levels greater than 1 were obtained close to the continent and attenuated seaward. This biomass inversion compounds that observed for zooplankton relative to phytoplankton stocks (Fig. 4 and Supplementary Fig. 1). Model simulations do not provide any evidence of biomass inversions for the 10–100 g class relative to the 1–10 kg class (Supplementary Fig. 4b–d). However, a biomass inversion is simulated off West Antarctica for the 10–100 kg class, which represents large predatory pelagic and demersal fish (Supplementary Fig. 4e). Estimates based on acoustics, net observations and modelled target strengths of fish project that the biomass of SO mesopelagic fish (274–570 Mt) is around fourfold higher than previously thought[148] and suggest further biomass inversions between trophic levels.

The identification of trophic patterns will make it possible to link the stocks of higher trophic levels with their fluxes and to understand their contribution to the SO carbon cycle; however, further observational advances will first be required. For example, advances in tracking and habitat models are needed to provide insight into the prey fields of marine mammals[149]; bioacoustic sensors on marine mammals and improved acoustic measurements should be used to understand the structure of the mesopelagic ecosystems[150]; and remote-sensing measurements are needed to monitor the fate of phytoplankton biomass (chlorophyll fluorescence[142]). At the highest trophic levels, additional ecological insights have come from animal telemetry (that is, remote sensing using a tag secured to the animal[151]) and bio-logging (biota with remote-sensing loggers[152,153]) but these insights cannot yet be incorporated into models. Together, these approaches have provided insight into the biology of elusive (cryptic) marine predators, including patterns of habitat usage, migratory routes, foraging and reproductive hotspots and navigation[154]. Additionally, bio-loggers have helped to fill spatial and seasonal gaps[155,156] in data on the shallow coastal areas and polynyas, where the highest NPP is often recorded[51,128,157]. Despite these advances, a major effort will be needed to obtain comprehensive observational datasets that can be compared with those produced by FishMIP (Supplementary Fig. 3).

Dissolved organic carbon

NPP is also influenced by the release of DOC, which can either occur directly through the loss of phytoplankton photosynthate into the upper ocean owing to nutrient limitation[158], or indirectly through viral lysis[116,159] or sloppy feeding by grazers[158]. These DOC release pathways are associated with labile (highly reactive and recently produced or released by biota — on a timescale of hours) forms of DOC; however, most DOC stocks in the ocean are unreactive and little is known about how DOC is transformed from labile to refractory forms[160]. There are fewer DOC profiles or vertical sections for the SO than other basins[161]; however, measurements of DOC and its radiocarbon content[161] have revealed that deep-water DOC is 400–600 years old, and behaves conservatively (that is, has similar concentrations across the deep ocean owing to its long residence time). These findings suggest that DOC is transferred at depth from other ocean basins over long timescales.

Ship-based methods remain the best sampling platform for DOC because although DOC sensors (measuring coloured dissolved organic matter) have been deployed on profiling floats, they provide noisy signals and poor-quality observations[162]. Ship-based observations provide insight into potential connections between upper-ocean DOC production and its transfer into and subsequent transformation in the oceans' interior. For example, deep-water DOC profiles can be overlaid by conspicuous DOC signatures, of higher concentrations, from the upper ocean, which are linked to sea-ice retreat and the concurrent release of dissolved iron from melting sea ice[163]. This release of dissolved iron stimulates NPP; a proportion of this photosynthetically fixed carbon is then released as labile DOC. Such upper-ocean DOC transforms from labile to recalcitrant forms of DOC in the marginal ice zone[164]. There are potential feedbacks between these processes because sea ice is rich in iron-binding ligands compared to ice-free waters, which prevent iron being scavenged and removed from the upper ocean[165,166]. However, the amount of ligands released from meltwater in spring and summer is highly variable and potentially influenced by external uptake and supply mechanisms[61,167].

DOC signatures sampled in 2008 (low sea-ice retreat) and 2017 (high sea-ice retreat) (Fig. 5a,b)[163] reveal different patterns and magnitudes of iron-mediated DOC export into the SO interior. In 2008, enhanced concentrations were observed at depth (2–4 µmol C kg^{-1} above deep-water background concentrations). This observation can be explained by the presence of frontal upwelling-supplied iron, whereas the enhanced DOC observed in 2017 (2–6 µmol C kg^{-1} higher than deep-water background levels at >50° S) was likely to have been primarily caused by the supply of iron from sea-ice melt.

An estimated 8 Tg of carbon enters the upper SO as labile DOC each year[168]; insights are still emerging about the fate of this large carbon flux. A sophisticated chemical analysis of DOC released in the marginal ice zone[164] of East Antarctica suggests that DOC sea-ice melt is rapidly transformed by microbes into recalcitrant DOC that can be

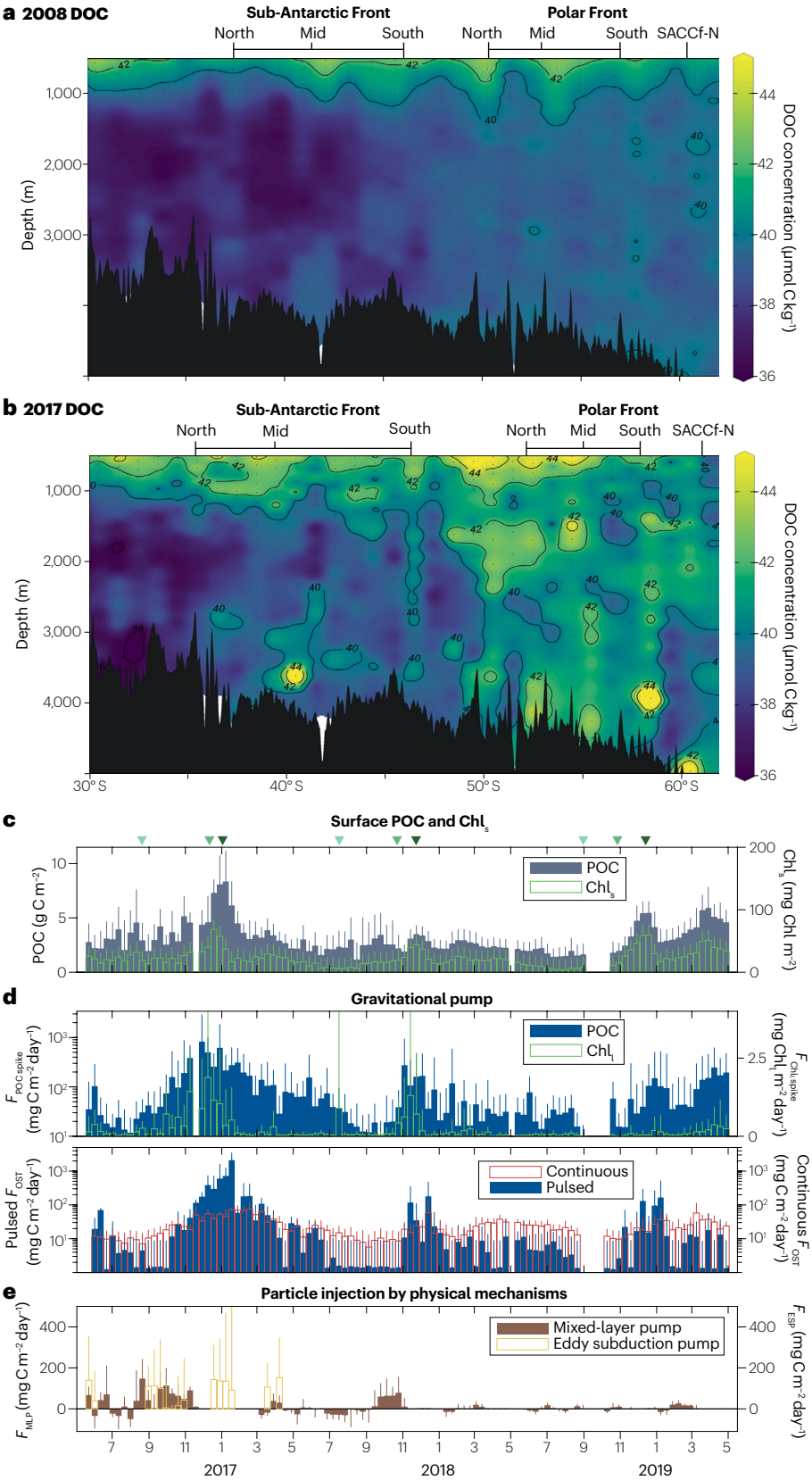

Fig. 5 | The influence of Southern Ocean productivity on dissolved organic carbon release and downward particle export flux. a, Dissolved organic carbon (DOC) export to depth in 2008 measured on Southern Ocean Pacific voyages (along 103° W West of Drake's Passage)[163]. SACCf-N, Southern Antarctic Circumpolar Current Front-North. **b**, As in **a**, but for 2017. **c**, Seasonality of surface ocean productivity (small-particle chlorophyll; Chl_s) and particulate organic carbon (POC) stocks. Inverted triangles denote the onset (left), climax (middle) and apex (right) of each annual bloom event[24]. **d**, Top, biological gravitational pump characterized by the downward flux of POC ($F_{POC\ spike}$) and large-particle chlorophyll ($F_{Chl\ spike}$). Bottom, the continuous and pulsed flux of sinking particles measured with an optical sediment trap (OST). **e**, Particle injection by the mixed-layer pump (F_{MLP}) and the eddy subduction pump (F_{ESP}) based on biogeochemical Argo float data[24]. The error bars in **c**–**e** represent the interquartile range. Conspicuous increases in subsurface concentrations (DOC) and export pulses (POC) denote the influence of surface productivity events on carbon dynamics in the oceans' interior. Parts **a** and **b** are reprinted from ref. 163 CC BY 3.0 https://creativecommons.org/licenses/by/3.0/). Parts **c**–**e** are reprinted from ref. 24, Springer Nature Ltd.

a Biological carbon pump metrics and air–sea flux for natural CO_2

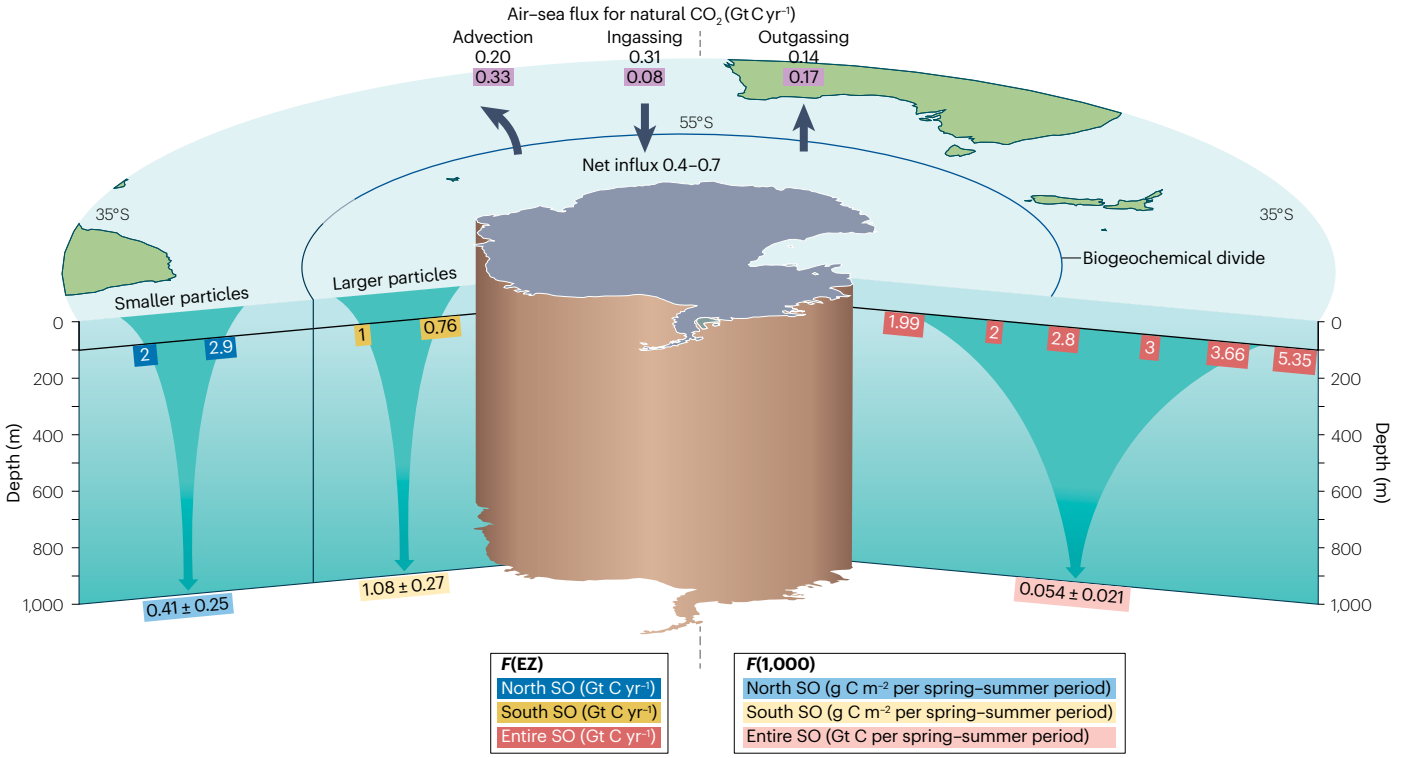

b Physical and biogeochemical processes

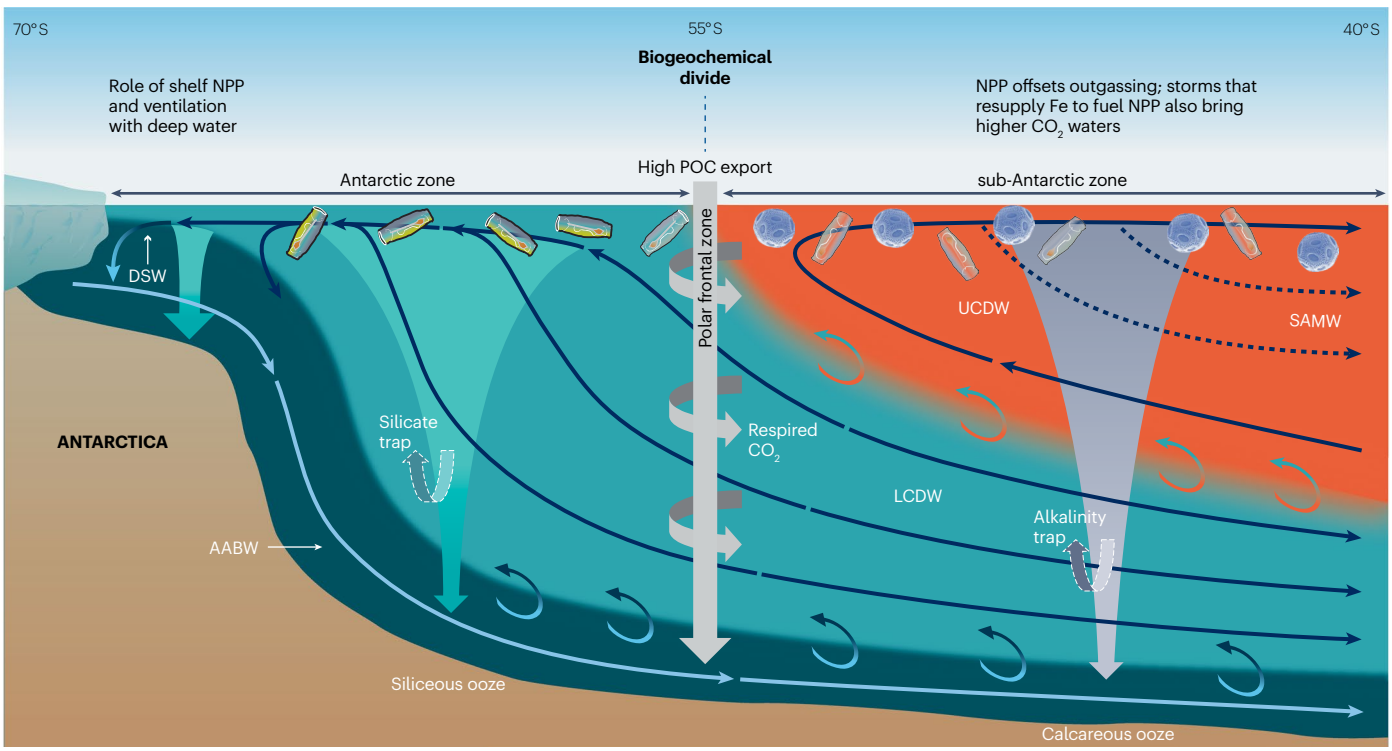

Fig. 6 | Southern Ocean circulation and biological processes driving the carbon cycle. a, Estimates of the annual export flux *F*(EZ) North and South of the biogeochemical divide[4,190] and for the entire Southern Ocean (SO)[4,190,191,245,246], as well as the flux at 1,000 m *F*(1,000) for the austral spring–summer period for the same regions[171,191]. Advection, ingassing and outgassing of natural CO_2 for 1990–2000 (purple shaded) and 2000–2010 (black) (ref. 5) as well as the net carbon influx[3,178] are also indicated. **b**, Schematic of idealized, zonal-mean overturning circulation, including main water masses (Antarctic Bottom Water (AABW), dark blue; Lower Circumpolar Deep Water (LCDW), light blue; Upper Circumpolar Deep Water (UCDW), orange; sub-Antarctic mode water (SAMW), dashed blue arrows; Dense Shelf Water (DSW), dark blue); the biogeochemical divide at the polar frontal zone, which is responsible for high particulate organic carbon (POC) export (light grey arrow); and dominant biomineralizing (ballasting) phytoplankton, which drive the carbonate pump (dark grey arrow) and the silicate trap (turquoise arrow). CO_2 outgassing in the SO is offset by net primary production (NPP) and the biological carbon pump and it is limited by calcification and the carbonate pump.

transported to depth on long timescales (years or more), representing a potentially large carbon sink. Additionally, the role of viral lysis in supplying DOC to SO surface waters has yet to be explored; however, field-based measurements of carbon flows and phytoplankton suggest that it has a major influence on NPP[159,169] in several SO provinces. Clearly, further research is required to understand the relative role of DOC as a long-term fate for the carbon from NPP.

Downward particle export

NPP can also be directly exported out of the upper ocean by the biological gravitational pump (BGP) or by physically mediated particle pumps that inject phytoplankton cells into the subsurface ocean[20,149] (Fig. 5c–e). Observational evidence of the functioning of the BGP in the SO during era 3 provides a diverse range of findings with no clear trends. For example, multi-float profiles in conjunction with a proxy for the fate of chlorophyll stocks[142] indicate that herbivory rather than direct export dominates the annual productivity cycle in the polar SO. However, glider-based observations in the Atlantic sector of the SO[170] revealed periods of high-efficiency export of NPP as pulses of phytoplankton POC transferred at depth, providing evidence that direct algal sinking could be important on shorter timescales. In one of the most comprehensive studies to date, distinctive patterns in export efficiency were observed in BGC-Argo profiles that coincided with six environments[171] including sea-ice cover, location of oceanic fronts and a proxy for iron supply. The patterns indicated that the efficiency of particle export flux increased with latitude and was driven by changes in the phytoplankton community structure (that is, more diatoms) and increasing particle size. High POC export efficiency linked to phytoplankton blooms was also reported for three coastal polynyas in East Antarctica[172]. A multi-year record of float observations[24] also revealed export flux pulses that are coupled with upper ocean phytoplankton processes (Fig. 5c–e).

Phytoplankton can also be transported out of the surface ocean by injection pumps such as the mixed-layer pump (in which particles are exported by detrainment) or eddy subduction pump (in which particles are injected along sloping isopyncals associated with the eddy fine structure)[162]. The downward injection of phytoplankton by the eddy subduction pump to depths of several hundred metres was observed by gliders in the North East Atlantic and extrapolated to the SO[173]. Simulations estimate that the eddy subduction pump could contribute a POC export flux equivalent to up to 50% of POC export from the BGP[173]. However, float-based observations found that the eddy subduction pump contributed only 1% of POC export[85] in the SO but that it contributed up to 40% of the magnitude of the BGP during summer events. Additionally, multi-year cycles of float data indicate that the seasonality of the eddy subduction pump and of the mixed-layer pump is different from that of the BGP[24], suggesting that phytoplankton could be directly injected to depth during other seasons (Fig. 5c–e).

In addition to physically mediated injection pumps, biologically modulated pumps such as the Mesopelagic Migrant Pump can transform phytoplankton across multiple trophic levels via grazing and then export this carbon to depth during diurnal vertical migration. Additionally, the seasonal migration of mesozooplankton to depth drives a downward POC flux — known as the seasonal lipid pump (in which carbon is actively transported as storage lipids below the permanent pycnocline). The Mesopelagic Migrant Pump could transport up to 50 Mt POC annually. When the faecal POC export (39 Mt for krill in the marginal ice zone[174]) and the seasonal lipid pump are considered together, they have the potential to make major contributions to downward carbon export. Observations of two seasonally migrating copepods[175] yield seasonal lipid pump estimates of 2.5–3.7 g C m^{-2} yr^{-1} (*Neocalanus tonsus*) and 0.1–0.5 g C m^{-2} yr^{-1} (*Calanoides acutus*) of injected dissolved inorganic carbon. A SO-wide extrapolation based on sub-Antarctic datasets gives an annual seasonal lipid pump export of 120–180 Mt (compared with BCP of about 3.2 Gt annually[4]). Cumulative estimates that combine the contributions of the physically and biologically mediated pumps that comprise the BCP are needed to refine estimates of the SO carbon cycle.

Biologically mediated processes

The partitioning of NPP into pathways by which phytoplankton carbon is transferred to other pools (such as grazer biomass and DOC) and fluxes (for example, downward particle export through the BCP) has a major influence on SO biogeochemistry. These fluxes are modified by ocean circulation and by microbes and zooplankton at depth, which attenuate the downward POC flux. Four influential biological processes that help to drive the SO carbon cycle are discussed here.

NPP and atmospheric CO_2 influx

NPP affects the meridional pattern of CO_2 uptake in the SO by photosynthetically fixing carbon and hence opposing CO_2 losses driven by temperature-related changes in solubility and the winter resupply of CO_2 to the surface ocean from the atmosphere or the upward mixing of carbon-rich waters from below[20,176]. Specifically, NPP helps to offset CO_2 outgassing associated with upwelling carbon-rich deep waters[177], turning the entire SO into a net CO_2 sink of about 0.4 Gt C yr^{-1} (based on measurements from tens of floats throughout 2014–2021)[178] to 0.7 Gt C yr^{-1} (based on observations and multiple global biogeochemical models for 1998–2018)[3] (Fig. 6a). In productive regions, the seasonal NPP cycle reduces the surface dissolved inorganic carbon concentration in summer and drives influx of atmospheric CO_2 (refs. 179–181). However, in the regions of mode water formation, deep mixing in autumn and winter facilitates a return to near-equilibrium with the atmosphere, or modest CO_2 efflux[3,20,182]. In Antarctic coastal regions, where waters are seasonally ice-covered, the brief, but intense, biologically mediated CO_2 uptake through NPP in summer[183] is followed

by the growth of sea ice, which effectively caps the water column in autumn and suppresses CO_2 outgassing in winter[182].

In less productive iron-limited waters, or those with seasonal silicate limitation, the offsetting of CO_2 outgassing in the upper cell is reduced owing to lower rates of NPP[80,177]. CO_2 outgassing through the upper cell was estimated to be about 0.4 Gt C yr^{-1} (refs. 80,177), but factors such as the Southern Annular Mode and physical events that communicate with the subsurface ocean such as storms could introduce interannual uncertainty. For example, a positive Southern Annular Mode has driven an increase and poleward contraction of westerly winds, leading to enhanced CO_2 outgassing[65,184]; however, such outgassing is also partially compensated for by an increase in NPP and hence particle export[2]. Ocean warming is expected to enhance stratification, which will limit outgassing but also potentially diminish NPP by isolating nutrients at depth[139,185,186]; however, this effect might not apply to large regions of the SO. Storm events[30] and vertical fluxes associated with eddies[187] could resupply iron to the upper ocean and enhance NPP. However, such communication with subsurface strata, often to depths of 200 m (ref. 188), will also entrain waters with higher dissolved inorganic carbon[55]. Thus, the stoichiometry of dissolved inorganic carbon to dissolved iron in the underlying waters will determine whether such entrainment represents a net increase (whereby outgassing exceeds iron-enhanced NPP) or decrease in CO_2 outgassing.

The biological carbon pump

The BCP is the downward flux of POC out of surface waters, which can be attenuated by mesopelagic biota seeking nutrition and influenced by oceanic circulation. Inverse-modelling based estimates of the BCP in the SO suggest annual exports of 3 Gt in regions above 30° S and 1 Gt in regions above 50° S (ref. 4). These estimates suggest that the SO makes a disproportionately large contribution to global downward POC export (around 10 Gt; ref. 162) despite the widespread iron limitation of NPP in the SO[189].

This regional export estimate has since been reassessed using float-based measurements. The annual export by the BCP has been estimated as 3.9 Gt, based on calculations of the net community production (a proxy for export flux) from dissolved oxygen profile time-series measurements in combination with a simple conversion factor (a constant respiratory quotient[190]). However, it is unknown to what extent net community production accounts for carbon injected by particle pumps. Additionally, the seasonal ice zone was not considered in regions where profiling float coverage is relatively poor. Basin-scale POC estimates have also been obtained using measurements from BGC-Argo floats (5.35 Gt C yr^{-1})[191] as well as measurements from more than 60 floats and over 100 ships (2.80 ± 0.28 Gt C yr^{-1})[178]. These estimates are of a similar order to modelled estimates[4] (Fig. 6a), which again raises the issue of how this large flux can be sustained by a region in which the magnitude of NPP is low owing to iron limitation. Model simulations suggest that increased numbers of large-sized, fast sinking particles and reduced remineralization rates in the SO could increase the efficiency of the transfer of particles into the oceans' interior[192].

A reciprocal effect of the BCP and the vertical attenuation of POC flux is the build-up of dissolved inorganic carbon at depth owing to respiration and remineralization of POC. This subsurface respired carbon inventory, which is also enhanced by the subsurface transport of respired CO_2 from other basins, is often re-ventilated because much of the SO carbon cycle is determined by ocean circulation and biological processes. This re-ventilation leads to CO_2 outgassing[177], and changes in the magnitude of respired CO_2 are important in the carbon cycle in the geological past[193]. Dissolved oxygen time-series from profiling floats in tandem with a respiratory quotient[190] have been used to assess depth-dependent patterns in POC remineralization[170] (driven by microbes and zooplankton) and the build-up of respired CO_2. These measurements found that across the basin, most of the remineralization occurs at depths of 100–500 m, with about 14% occurring below 500 m where the flux was 0.12 Gt C yr^{-1} (ref. 190).

Observations from multiple floats indicate that vertical patterns in POC remineralization, driven by bacterial respiration, are responsible for most of the variability in the SO POC inventory at depth, rather than the magnitude of POC export[191]. Other float-based measurements have explored patterns in flux attenuation and their drivers by comparing the POC flux to depths of 1,000 m with the particle characteristics of the upper ocean[171]. These measurements estimated a mean austral spring and summer POC flux of large particles of 0.054 ± 0.021 Gt for the basin at a depth of 1,000 m over a 180-day phytoplankton productive season (Fig. 6a). Thus, the attenuation of POC flux returns a large proportion of the carbon to the inventory of respired CO_2 (Fig. 6a). Despite this large CO_2 inventory, and its potential to outgas, float-based measurements based on a tracer budget approach[178] indicate that the SO would not be a carbon sink (0.43 ± 0.14 Gt C yr^{-1}) without the joint contribution of the BCP and DOC export (2.80 ± 0.28 Gt C yr^{-1}) compared with carbon lost through physical efflux (2.10 ± 0.24 Gt C yr^{-1}) and the particulate inorganic carbon counter-pump (0.27 ± 0.21 Gt C yr^{-1}).

The role of NPP in shelf seas

The timing and magnitude of NPP on the shelves that surround Antarctica is strongly linked to light and nutrient availability, which are both related to water-column stratification and sea-ice cover[14,15]. The POC formed by phytoplankton in summer when light and nutrients are abundant can either be recycled or exported to depth where it is remineralized to CO_2 (ref. 194). However, in regions of dense shelf water formation (such as coastal polynyas), these CO_2-rich waters can be transported offshore, efficiently transferring both natural and anthropogenic CO_2 to the deep ocean[183,195]. Unfortunately, the processes characterizing shelf areas[196] (such as ice-shelf cavities[197]) are not comprehensively represented by models that provide large-scale estimates of air–sea CO_2 fluxes[183,195], owing to a lack of observations and modelling priorities.

Despite being small relative to the entire SO basin, the shelf seas could make important contributions to the SO carbon cycle. In the West Antarctic Peninsula region, changes to sea-ice dynamics have caused dramatic several-fold increases in summer CO_2 uptake. However, continued warming and ice loss are expected to weaken this ocean carbon sink in the coming decades[182,198]. Since 2010, on the relatively narrow East Antarctic continental shelves reconfigurations of the ice environment (such as glaciers, icebergs and polynyas) have been linked to short-term increases in the net community production and oceanic CO_2 uptake[199]. However, the increased input of glacial meltwater is expected to reduce deep water formation[196] despite increases in NPP caused by the release of iron from meltwater[61,200]. These changes could have detrimental implications for the transfer of anthropogenic CO_2 to depth and offshore from East Antarctic shelf seas[201].

Calcification counters CO_2 uptake

Calcification by coccolithophores (and other biota) and the subsequent downward flux of $CaCO_3$ within the GCB traps alkalinity in the SO (Fig. 6b). This calcification strips alkalinity from northward-flowing surface waters in the upper cell leading to the deposition of $CaCO_3$ in the deep layers of the sub-Antarctic zone through $CaCO_3$ dissolution

(Fig. 6b). This process feeds into the upwelling at the Antarctic divergence (between the Polar Front and the sea-ice edge)[202], reducing CO_2 outgassing of pre-industrial carbon[105]. Calcification rates in the GCB decreased by 4% during 1998–2014 (ref. 203) owing to ocean acidification, implying that less alkalinity is trapped in the SO and is instead allowed to escape northwards, which allows the global ocean to absorb more CO_2 (ref. 202).

Calcification reduces surface water alkalinity, and thus decreases the ability of the ocean to absorb CO_2 from the atmosphere and counteracts the uptake of CO_2 through the BCP[204]. The strength of this counter-effect depends on the composition of calcifying biota, with a stronger effect when calcification is dominated by heterotrophic organisms[205,206] rather than autotrophic organisms (coccolithophores). For example, when calcifying biota are dominated by shelled pteropods or foraminifera, CO_2 drawdown is countered by 17% (ref. 205) or 6–32% (ref. 206), respectively, compared with 6–10% (refs. 205,207,208) when coccolithophores dominate. Integrated over the SO, the carbonate pump can counter CO_2 uptake by the BCP by 11% (estimated range 4–17%; ref. 178), which is close to the global median value of 7% (ref. 209). Techniques to detect such calcifying organisms remotely, such as image analysis (Underwater Vision Profiler version 6, UVP6) for heterotrophs and metazoans, or ocean-colour satellite (reflectance) measurements and cross polarised transmissionmeters[206] for autotrophs, will continue to improve the accuracy of estimates of this counter-effect.

Uncertainty in projections of biological processes

In model projections, varying degrees of uncertainty exist regarding how biological processes that contribute to the SO carbon cycle will change in the coming decades. For example, future changes in the magnitude of NPP in the SO (and hence its influence on CO_2 uptake)[119,210] are better understood than future changes to the POC export flux[140]. For NPP projections, multiple environmental factors must be considered, including changes in iron supply, mixed-layer depth, sea-ice melt and westerly wind belts[211]. The effect of altering these individual drivers, along with their interplay with one another, remains poorly understood[212]. Additionally, the lack of understanding of the many factors that drive downward export flux — such as zooplankton grazing[143], the inventory of respired CO_2, the role of shelf seas in sequestering POC, and the wider basin-scale role of the alkalinity trap — means that projections of these key SO carbon cycle processes are poorly constrained[140,144]. For example, major changes in NPP are projected in shelf seas[119], but the interplay of these changes with concurrent changes in the physical circulation near Antarctica and in sea-ice dynamics[177] introduces major uncertainties[195].

Summary and future perspectives

Improvements in observations of SO biogeochemistry and ecology using a combination of robotic profiling floats, animal telemetry, uncrewed surface vehicles and gliders to complement the roles of ships and satellites have made it possible to better resolve the contribution of biota to the regional carbon cycle (Supplementary Fig. 5). For example, multi-year float deployments have provided highly resolved water-column observations in the upper 2 km of the ocean's interior, which have refined estimates of POC export flux and its attenuation with depth[171,178]. These measurements have also provided insight on changes in the midwater oxygen inventory[190], revealing where in the water column particle remineralization is occurring. However, several major gaps remain regarding marine chemical observations, in particular for dissolved iron and DOC. Given the pivotal role of iron supply in determining NPP patterns[189] and the potential contribution of DOC to the regional carbon cycle, it will be important to improve projections of iron supply and DOC dynamics. Thus, multi-faceted advances in observing technologies will be needed to continue to improve understanding of SO biota and their role in the regional carbon cycle (Fig. 6a). These advances can be divided into the following categories: optimize technologies to enable more observations to extend coverage; improve understanding and accuracy of current observations that indirectly sample the carbon cycle; devise new sensors; and develop robust proxies using single or multiple sensor datasets[142] for observations (Supplementary Table 1).

Although there has been progress in developing remote trace-metal clean water sampling on moorings[213], proxies for iron stress (photophysiology) or supply (such as hydrothermal tracers) that can be measured remotely are needed. Some preliminary proxies exist (such as bio-optical metrics[210] for phytoplankton iron stress) but improvements are required. The bio-optical properties of the

Glossary

Biogeochemical Argo
(BGC-Argo). An international study using floats to measure oxygen, nitrate, pH, fluorescence, suspended particles and downwelling irradiance in addition to standard oceanographic variables such as temperature, salinity, and pressure measured by Argo floats.

Biogeochemical Southern Ocean State Estimate
(B-SOSE). A model estimate of circulation and biogeochemistry that assimilates output from Argo floats, hydrographic cruises and satellites.

Biological carbon pump
(BCP). The transport of a small but substantial proportion of photosynthetically fixed carbon through the gravitational settling of particles or the injection of particles by physical or biological processes to the ocean's interior.

Biological gravitational pump
(BGP). A component of the biological carbon pump that focuses on passively sinking material.

Fisheries and Marine Ecosystem Model Intercomparison Project
(FishMIP). A project that aims to understand and project long-term effects of climate change on fisheries and marine ecosystems and inform policy.

Great Calcite Belt
(GCB). A circumpolar band of high calcite concentrations in the water column between the circumpolar subtropical and polar fronts caused by a dominance of coccolithophores.

NASA Plankton, Aerosol, Cloud, ocean Ecosystems project
(NASA PACE). A project that aims to improve NASA's satellite records of global ocean biology, aerosols and clouds through hyperspectral measurements (5 nm resolution). PACE launched in February 2024.

Net primary production
(NPP). The difference between the energy fixed by autotrophs such as phytoplankton and their respiration. NPP drives phytoplankton growth and increases in phytoplankton stocks, that is, high NPP leads to high chlorophyll concentrations.

Underwater Vision Profiler version 6
(UVP6). A miniaturized and low-price version of the UVP5, which was designed to be attached to floats and acquire float profiles of plankton and particle images.

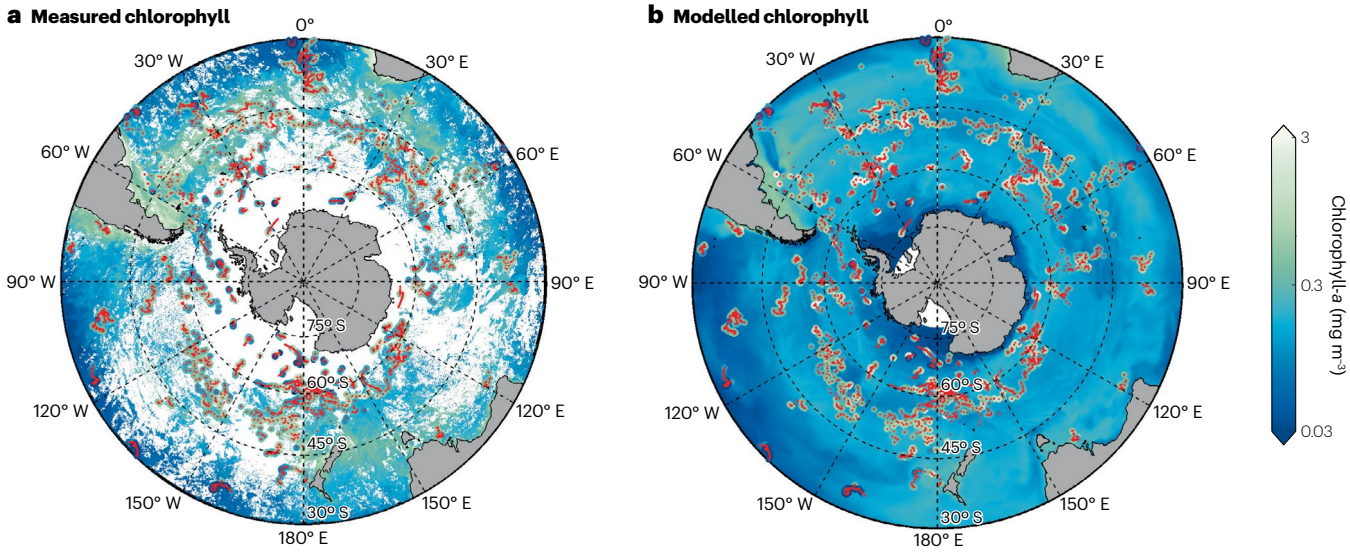

Fig. 7 | Integrating measured and modelled biogeochemical properties. **a**, October 2019–September 2020 mean annual surface colour from the Ocean Colour Climate Change Initiative (OC-CCI) and surface layer (top 30 m) chlorophyll-*a* concentrations from biogeochemical Argo floats (in the locations shown by the red dots). **b**, As in **a**, but for the mean annual surface layer (top 30 m) chlorophyll-*a* from the biogeochemical Southern Ocean state estimate (B-SOSE[217]) model (modified from the BLING model; Supplementary Fig. 6). B-SOSE is a powerful illustration of how multiple observational datasets from different platforms can be coupled with model simulations to provide a 4D regional ocean observatory.

SO have always been difficult to measure with satellite oceanography, owing to their increased complexity relative to other ocean basins[214]. To improve regional algorithms for ocean colour, better linkages with photo-physiology will be needed[215,216] to reveal unique physiological strategies employed in the extreme SO environment. New sensors are also being developed for satellites, for example, the NASA Plankton Aerosol Clouds Ecosystems Project (NASA PACE) hyperspectral satellite.

Advances in observations should be accompanied by the integration of the obtained datasets into ocean models[217]. However, the sampling frequency of the measurements can influence the extracted regional carbon budgets, which can cause the estimated magnitude of the carbon sink to vary between studies[141,218]. For example, SO carbon budgets for 1998–2018 calculated using observation-based products and a global biogeochemical model[3] yield a larger estimate of net CO_2 uptake[20,219] than budgets based on measurements from a relatively small number of floats during 2014–2021 (ref. 178). It is likely that this divergence is caused by differences in the sampling frequency and period between the two studies.

As the number of observations increases, it will also become increasingly challenging to merge datasets from different sensors, for example, combining data from satellites and floats to improve regional estimates of NPP. It will also be important to better understand the limitations of some observational technologies relative to others and to reappraise the important data-gathering and validation role of research vessels[220]. It is likely that a wide range of modelling approaches will be needed to handle such disparate data suites from those generated on research ships to remote sensing. Such approaches could include simple mechanistic models to complex multiple plankton functional models[204] and data-assimilating dynamic models[217], along with models incorporating sub-processes solved through artificial intelligence[221,222]. The use of machine learning in conjunction with data-driven approaches and data assimilation could represent a way forward (for example, such approaches have been used to map the surface ocean partial pressure of CO_2 and air–sea CO_2 fluxes[223]).

Although these developments in observational technologies and capabilities will improve the quality and scale of observations, parallel developments in data synthesis, integration and model parameterizations will also be needed to better understand the role of biota in the SO carbon cycle. The Biogeochemical Southern Ocean State Estimate[217] (B-SOSE) is an example of a 4D SO observatory that combines multiple physical and chemical observations from vessels and BGC-Argo floats with previous simulations. Additionally, B-SOSE has the structure in place to further assimilate satellite and BGC-Argo chlorophyll observations as they are acquired (Fig. 7). This approach can also include observations from bio-logging. These modelling results can then be used to further guide observational needs. For instance, results from B-SOSE demonstrate that, on timescales exceeding 90 days, a minimum of 100 optimally spaced BGC-Argo floats will be required to monitor and constrain SO carbon and heat fluxes[223]. Such recommendations from B-SOSE will inform future deployment strategies of floats and identify key deliverables to reduce uncertainties in the SO carbon cycle.

Another possible approach to integrating models and observations from multiple sources is the estimation of biogeochemical parameters in ecosystem models using data assimilation[224] (Supplementary Fig. 6). Observations can be used to iteratively compare hundreds of model simulations with small variations in parameter values, to obtain a set of parameters that best represents the observed variables[225]. This approach offers advantages over the manual tuning of models, because the estimation process can provide insight into which processes are critical in determining the model's behaviour[226,227]. Data assimilation for state and parameter estimation will not only improve the capabilities of models but can also guide the selection of an appropriate level of biogeochemical model complexity for the region[228] and the identification

of time- and/or spatially varying parameters. Such developments will require a balance between the processes that researchers want to include in models and those that can be properly constrained by observations. However, such observational constraints remain sparse. In particular, foodweb dynamics, including zooplankton grazing and other phytoplankton fates, are often poorly constrained in regional models[228,229]. We anticipate that the assimilation of zooplankton observations and improved representation of grazing fluxes will improve estimates of zooplankton biomass, NPP and export[230–232].

As the observation network in the SO expands, improvements in model representation, skill and forecasting capabilities can be expected. Within the next decade, we envisage that improvements will be made in reproducing the SO mesoscale, which is becoming increasingly well constrained ocean-wide; in determining accurate fluxes, particularly by reducing biases in air–sea exchanges over the SO; and in quantifying carbon and nutrient inventories. Short- and long-term model projections will become more accurate as a diverse and sustained network of biological observations is maintained. 4D observatories will make it possible to exploit the potential of current observations and those from ongoing sensor technology developments, to better understand the modes of control on SO biota, and in turn the dynamic (carbon) biogeochemical provinces of the upper ocean and its interior.

Data availability

The data for the FishMIP marine ecosystem models and the two Earth system models, IPSL-CM6A-LR and GFDL-ESM4, used to make Fig. 4c and d and Supplementary Figs. 1–4, are available through the ISIMIP repository (https://data.isimip.org/; https://doi.org/10.48364/ISIMIP.575744.4).

Code availability

The code used to produce Fig. 4, and Supplementary Figs. 1–4 is available at https://github.com/Fish-MIP/Extract_SouthernOcean.

Published online: 11 April 2024

References

1. Talley, L. Closure of the global overturning circulation through the Indian, Pacific, and Southern oceans: schematics and transports. *Oceanography* **26**, 80–97 (2013).
2. Gruber, N. et al. Trends and variability in the ocean carbon sink. *Nat. Rev. Earth Environ.* **4**, 119–134 (2023).
3. Hauck, J. et al. The Southern Ocean Carbon Cycle 1985–2018: mean, seasonal cycle, trends, and storage. *Glob. Biogeochem. Cycles* **37**, e2023GB007848 (2023).
4. Schlitzer, R. Carbon export fluxes in the Southern Ocean: results from inverse modeling and comparison with satellite-based estimates. *Deep. Sea Res. II* **49**, 1623–1644 (2002).
5. DeVries, T. & Weber, T. The export and fate of organic matter in the ocean: new constraints from combining satellite and oceanographic tracer observations. *Glob. Biogeochem. Cycles* **31**, 535–555 (2017).
6. Nissen, C. & Vogt, M. Factors controlling the competition between *Phaeocystis* and diatoms in the Southern Ocean and implications for carbon export fluxes. *Biogeosciences* **18**, 251–283 (2021).
7. Marinov, I., Gnanadesikan, A., Toggweiler, J. R. & Sarmiento, J. L. The Southern Ocean biogeochemical divide. *Nature* **441**, 964–967 (2006).
8. Landschützer, P. et al. The reinvigoration of the Southern Ocean carbon sink. *Science* **349**, 1221–1224 (2015).
9. Le Quéré, C. et al. Saturation of the Southern Ocean CO_2 sink due to recent climate change. *Science* **316**, 1735–1738 (2007).
10. Sarmiento, J. L., Gruber, N., Brzezinski, M. A. & Dunne, J. P. High-latitude controls of thermocline nutrients and low latitude biological productivity. *Nature* **427**, 56–60 (2004).
11. El-Sayed, S. Z. Primary productivity and estimates of potential yields of the Southern Ocean. In *Polar Research* (Routledge, 1978).
12. Holm-Hansen, O., El-Sayed, S., Franchesini, G. A. & Cuhel, R. L. Primary production and the factors controlling phytoplankton growth in the Antarctic seas. In *Proceedings of SCAR Symposium in Antarctic Biology* (ed. Llano, G. A.) 11–50 (Wiley, 1977).
13. Smith, W. O., Keene, N. K. & Comiso, J. C. Interannual variability in estimated primary productivity of the Antarctic marginal ice zone. In *Antarctic Ocean and Resources Variability* (ed. Sahrhage, D.) 131–139 (Springer, 1988).
14. Smith, W. O. & Nelson, D. M. Importance of ice edge phytoplankton production in the Southern Ocean. *BioScience* **36**, 251–257 (1986).
15. Arrigo, K. R., Van Dijken, G. L. & Bushinsky, S. Primary production in the Southern Ocean, 1997–2006. *J. Geophys. Res.* **113**, C08004 (2008).
16. Arrigo, K. R., Worthen, D., Schnell, A. & Lizotte, M. P. Primary production in Southern Ocean waters. *J. Geophys. Res. Ocean.* **103**, 15587–15600 (1998).
17. Moore, J. K. & Abbott, M. R. Phytoplankton chlorophyll distributions and primary production in the Southern Ocean. *J. Geophys. Res. Ocean.* **105**, 28709–28722 (2000).
18. Sarmiento, J. L. et al. The Southern Ocean carbon and climate observations and modeling (SOCCOM) project: a review. *Prog. Oceanogr.* **219**, 103130 (2023).
19. Gray, A. R. The four-dimensional carbon cycle of the Southern Ocean. *Annu. Rev. Mar. Sci.* **16**, https://doi.org/10.1146/annurev-marine-041923-104057 (2024).
20. Gray, A. R. et al. Autonomous biogeochemical floats detect significant carbon dioxide outgassing in the high-latitude Southern Ocean. *Geophys. Res. Lett.* **45**, 9049–9057 (2018).
21. Sutton, A. J., Williams, N. L. & Tilbrook, B. Constraining Southern Ocean CO_2 flux uncertainty using uncrewed surface vehicle observations. *Geophys. Res. Lett.* **48**, https://doi.org/10.1029/2020GL091748 (2021).
22. Ardyna, M. et al. Hydrothermal vents trigger massive phytoplankton blooms in the Southern Ocean. *Nat. Commun.* **10**, 2451 (2019).
23. Baldry, K., Strutton, P. G., Hill, N. A. & Boyd, P. W. Subsurface chlorophyll-*a* maxima in the Southern Ocean. *Front. Mar. Sci.* **7**, 671 (2020).
24. Lacour, L., Llort, J., Briggs, N., Strutton, P. G. & Boyd, P. W. Seasonality of downward carbon export in the Pacific Southern Ocean revealed by multi-year robotic observations. *Nat. Commun.* **14**, 1278 (2023).
25. Bisson, K. M. & Cael, B. B. How are under ice phytoplankton related to sea ice in the Southern Ocean? *Geophys. Res. Lett.* **48**, https://doi.org/10.1029/2021GL095051 (2021).
26. Horvat, C., Bisson, K., Seabrook, S., Cristi, A. & Matthes, L. C. Evidence of phytoplankton blooms under Antarctic sea ice. *Front. Mar. Sci.* **9**, https://doi.org/10.3389/fmars.2022.942799 (2022).
27. Arteaga, L. A., Boss, E., Behrenfeld, M. J., Westberry, T. K. & Sarmiento, J. L. Seasonal modulation of phytoplankton biomass in the Southern Ocean. *Nat. Commun.* **11**, 5364 (2020).
28. Ardyna, M. et al. Delineating environmental control of phytoplankton biomass and phenology in the Southern Ocean: phytoplankton dynamics in the SO. *Geophys. Res. Lett.* **44**, 5016–5024 (2017).
29. Sallée, J.-B., Llort, J., Tagliabue, A. & Lévy, M. Characterization of distinct bloom phenology regimes in the Southern Ocean. *ICES J. Mar. Sci.* **72**, 1985–1998 (2015).
30. Prend, C. J. et al. Sub-seasonal forcing drives year-to-year variations of southern ocean primary productivity. *Glob. Biogeochem. Cycles* **36**, 2022GB007329 (2022).
31. Nicholson, S.-A., Lévy, M., Llort, J., Swart, S. & Monteiro, P. M. S. Investigation into the impact of storms on sustaining summer primary productivity in the Sub-Antarctic Ocean: storms sustain summer primary production. *Geophys. Res. Lett.* **43**, 9192–9199 (2016).
32. Uchida, T. et al. Southern Ocean phytoplankton blooms observed by biogeochemical floats. *J. Geophys. Res. Ocean.* **124**, 7328–7343 (2019).
33. Hart, T. J. On the phytoplankton of the south-west Atlantic and the Bellingshausen Sea, 1929–31. *Discovery Reports* Vol. 8, 1–268 (Califrnia Univ. Press, 1934).
34. Mitchell, B. G., Brody, E. A., Holm-Hansen, O., McClain, C. & Bishop, J. Light limitation of phytoplankton biomass and macronutrient utilization in the Southern Ocean. *Limnol. Oceanogr.* **36**, 1662–1677 (1991).
35. Banse, K. Does iron really limit phytoplankton production in the offshore subarctic Pacific? *Limnol. Oceanogr.* **35**, 772–775 (1990).
36. Martin, J. H. Glacial–interglacial CO_2 change: the iron hypothesis. *Paleoceanography* **5**, 1–13 (1990).
37. Boyd, P. W. et al. Atmospheric iron supply and enhanced vertical carbon flux in the NE subarctic Pacific: is there a connection? *Glob. Biogeochem. Cycles* **12**, 429–441 (1998).
38. de Baar, H. J. W. et al. Importance of iron for plankton blooms and carbon dioxide drawdown in the Southern Ocean. *Nature* **373**, 412–415 (1995).
39. Boyd, P. W. & Ellwood, M. J. The biogeochemical cycle of iron in the ocean. *Nat. Geosci.* **3**, 675–682 (2010).
40. Tagliabue, A. et al. Surface-water iron supplies in the Southern Ocean sustained by deep winter mixing. *Nat. Geosci.* **7**, 314–320 (2014).
41. Meskhidze, N., Nenes, A., Chameides, W. L., Luo, C. & Mahowald, N. Atlantic Southern Ocean productivity: fertilization from above or below? *Glob. Biogeochem. Cycles* **21**, GB2006 (2007).
42. Wagener, T., Guieu, C., Losno, R., Bonnet, S. & Mahowald, N. Revisiting atmospheric dust export to the Southern Hemisphere ocean: biogeochemical implications. *Glob. Biogeochem. Cycles* **22**, GB2006 (2008).
43. de Jong, J. et al. Iron in land-fast sea ice of McMurdo Sound derived from sediment resuspension and wind-blown dust attributes to primary productivity in the Ross Sea, Antarctica. *Mar. Chem.* **157**, 24–40 (2013).
44. Duprat, L. et al. Enhanced iron flux to antarctic sea ice via dust deposition from ice-free coastal areas. *J. Geophys. Res. Ocean.* **124**, 8538–8557 (2019).
45. Gassó, S. & Torres, O. Temporal characterization of dust activity in the central Patagonia Desert (years 1964–2017). *J. Geophys. Res. Atmos.* **124**, 3417–3434 (2019).

46. Tang, W. et al. Widespread phytoplankton blooms triggered by 2019-2020 Australian wildfires. *Nature* **597**, 370–375 (2021).
47. Weis, J. et al. Southern Ocean phytoplankton stimulated by wildfire emissions and sustained by iron recycling. *Geophys. Res. Lett.* **49**, e2021GL097538 (2022).
48. Perron, M. M. G., Proemse, B. C., Strzelec, M., Gault-Ringold, M. & Bowie, A. R. Atmospheric inputs of volcanic iron around Heard and McDonald Islands, Southern Ocean. *Environ. Sci. Atmos.* **1**, 508–517 (2021).
49. Alderkamp, A.-C. et al. Iron from melting glaciers fuels phytoplankton blooms in the Amundsen Sea (Southern Ocean): phytoplankton characteristics and productivity. *Deep. Sea Res. II* **71–76**, 32–48 (2012).
50. Hopwood, M. J. et al. Highly variable iron content modulates iceberg-ocean fertilisation and potential carbon export. *Nat. Commun.* **10**, 5261 (2019).
51. Moreau, S. et al. Sea ice meltwater and circumpolar deep water drive contrasting productivity in three Antarctic polynyas. *J. Geophys. Res. Ocean.* **124**, 2943–2968 (2019).
52. Sedwick, P. N. & DiTullio, G. R. Regulation of algal blooms in Antarctic shelf waters by the release of iron from melting sea ice. *Geophys. Res. Lett.* **24**, 2515–2518 (1997).
53. St-Laurent, P., Yager, P. L., Sherrell, R. M., Stammerjohn, S. E. & Dinniman, M. S. Pathways and supply of dissolved iron in the Amundsen Sea (Antarctica). *J. Geophys. Res. Ocean.* **122**, 7135–7162 (2017).
54. Nicholson, S. A. et al. Iron supply pathways between the surface and subsurface waters of the Southern Ocean: from winter entrainment to summer storms. *Geophys. Res. Lett.* **46**, 14567–14575 (2019).
55. Nicholson, S.-A. et al. Storms drive outgassing of CO_2 in the subpolar Southern Ocean. *Nat. Commun.* **13**, 158 (2022).
56. Lancelot, C. et al. Spatial distribution of the iron supply to phytoplankton in the Southern Ocean: a model study. *Biogeosciences* **6**, 2861–2878 (2009).
57. Lannuzel, D. et al. Iron in sea ice: review and new insights. *Elem. Sci. Anthr.* **4**, 000130 (2016).
58. Duprat, L. P. A. M., Bigg, G. R. & Wilton, D. J. Enhanced Southern Ocean marine productivity due to fertilization by giant icebergs. *Nat. Geosci.* **9**, 219–221 (2016).
59. Smith, K. L. Free-drifting icebergs in the Southern Ocean: an overview. *Deep. Sea Res. II* **58**, 1277–1284 (2011).
60. Boyd, P. W., Ibisanmi, E., Sander, S. G., Hunter, K. A. & Jackson, G. A. Remineralization of upper ocean particles: implications for iron biogeochemistry. *Limnol. Oceanogr.* **55**, 1271–1288 (2010).
61. Gerringa, L. J. A. et al. Iron from melting glaciers fuels the phytoplankton blooms in Amundsen Sea (Southern Ocean): iron biogeochemistry. *Deep. Sea Res. II* **71–76**, 16–31 (2012).
62. Ratnarajah, L., Nicol, S. & Bowie, A. R. Pelagic iron recycling in the Southern Ocean: exploring the contribution of marine animals. *Front. Mar. Sci.* **5**, 109 (2018).
63. Tovar-Sanchez, A., Duarte, C. M., Hernández-León, S. & Sañudo-Wilhelmy, S. A. Krill as a central node for iron cycling in the Southern Ocean. *Geophys. Res. Lett.* **32**, L11601 (2007).
64. Moreau, S. et al. Wind-driven upwelling of iron sustains dense blooms and food webs in the eastern Weddell gyre. *Nat. Commun.* **14**, 1303 (2023).
65. Lovenduski, N. S. & Gruber, N. Impact of the southern annular mode on Southern Ocean circulation and biology. *Geophys. Res. Lett.* **32**, L11603 (2005).
66. Reygondeau, G. et al. Dynamic biogeochemical provinces in the global ocean. *Glob. Biogeochem. Cycles* **27**, 1046–1058 (2013).
67. Boyd, P. W., Arrigo, K. R., Strzepek, R. & Van Dijken, G. L. Mapping phytoplankton iron utilization: insights into Southern Ocean supply mechanisms: Southern Ocean Fe utilization and supply. *J. Geophys. Res. Ocean.* **117**, C06009 (2012).
68. Carr, M.-E. et al. A comparison of global estimates of marine primary production from ocean color. *Deep. Sea Res. II* **53**, 741–770 (2006).
69. Bowie, A. R. et al. Biogeochemical iron budgets of the Southern Ocean south of Australia: decoupling of iron and nutrient cycles in the subantarctic zone by the summertime supply. *Glob. Biogeochem. Cycles* **23**, https://doi.org/10.1029/2009GB003500 (2009).
70. Boyd, P. W. et al. FeCycle: attempting an iron biogeochemical budget from a mesoscale SF 6 tracer experiment in unperturbed low iron waters. *Glob. Biogeochem. Cycles* **19**, GB4S20 (2005).
71. Coale, K. H. et al. Southern Ocean iron enrichment experiment: carbon cycling in high- and low-Si waters. *Science* **304**, 408–414 (2004).
72. Hoppe, C. J. M. et al. Iron limitation modulates ocean acidification effects on Southern Ocean phytoplankton communities. *PLoS One* **8**, e79890 (2013).
73. Martin, J. H., Fitzwater, S. E. & Gordon, R. M. Iron deficiency limits phytoplankton growth in Antarctic waters. *Glob. Biogeochem. Cycles* **4**, 5–12 (1990).
74. Smetacek, V. et al. Deep carbon export from a Southern Ocean iron-fertilized diatom bloom. *Nature* **487**, 313–319 (2012).
75. Browning, T. J., Achterberg, E. P., Engel, A. & Mawji, E. Manganese co-limitation of phytoplankton growth and major nutrient drawdown in the Southern Ocean. *Nat. Commun.* **12**, 884 (2021).
76. Latour, P. et al. Manganese biogeochemistry in the Southern Ocean, from Tasmania to Antarctica. *Limnol. Oceanogr.* **66**, 2547–2562 (2021).
77. McCain, J. S. P. et al. Cellular costs underpin micronutrient limitation in phytoplankton. *Sci. Adv.* **7**, eabg6501 (2021).
78. Wu, M. et al. Manganese and iron deficiency in Southern Ocean *Phaeocystis antarctica* populations revealed through taxon-specific protein indicators. *Nat. Commun.* **10**, 3582 (2019).
79. Lee, P. A. et al. Influence of vitamin B12 availability on oceanic dimethylsulfide and dimethylsulfoniopropionate. *Environ. Chem.* **13**, 293–301 (2015).
80. Mikaloff Fletcher, S. E. et al. Inverse estimates of the oceanic sources and sinks of natural CO_2 and the implied oceanic carbon transport. *Glob. Biogeochem. Cycles* **21**, GB1010 (2007).
81. Arrigo, K. R., Van Dijken, G. L. & Strong, A. L. Environmental controls of marine productivity hot spots around Antarctica. *J. Geophys. Res. Ocean.* **120**, 5545–5565 (2015).
82. Arrigo, K. R. & Van Dijken, G. Phytoplankton dynamics within 37 Antarctic coastal polynya systems. *J. Geophys. Res.* **108**, 3271 (2003).
83. Smith, W. O. & Gordon, L. I. Hyperproductivity of the Ross Sea (Antarctica) polynya during austral spring. *Geophys. Res. Lett.* **24**, 233–236 (1997).
84. Cornec, M. et al. Deep chlorophyll maxima in the Global Ocean: occurrences, drivers and characteristics. *Glob. Biogeochem. Cycles* **35**, e2020GB006759 (2021).
85. Acuña, J., López-Alvarez, M., Nogueira, E. & González-Taboada, F. Diatom flotation at the onset of the spring phytoplankton bloom: an in situ experiment. *Mar. Ecol. Prog. Ser.* **400**, 115–125 (2010).
86. Llort, J. et al. Evaluating Southern Ocean carbon eddy-pump from biogeochemical-Argo floats. *J. Geophys. Res. Ocean.* **123**, 971–984 (2018).
87. Tripathy, S. C. et al. Deep chlorophyll maximum and primary productivity in Indian Ocean sector of the Southern Ocean: case study in the subtropical and polar front during austral summer 2011. *Deep. Sea Res. II* **118**, 240–249 (2015).
88. Carranza, M. M. et al. When mixed layers are not mixed. Storm-driven mixing and bio-optical vertical gradients in mixed layers of the Southern Ocean. *J. Geophys. Res. Ocean* **123**, 7264–7289 (2018).
89. Legendre, L. et al. Ecology of sea ice biota: 2. Global significance. *Polar Biol.* **12**, 429–444 (1992).
90. Saenz, B. T. & Arrigo, K. R. Annual primary production in Antarctic sea ice during 2005–2006 from a sea ice state estimate. *J. Geophys. Res. Ocean.* **119**, 3645–3678 (2014).
91. Horner, R. et al. Ecology of sea ice biota: 1. Habitat, terminology, and methodology. *Polar Biol.* **12**, 417–427 (1992).
92. Van Leeuwe, M. A. et al. Microalgal community structure and primary production in Arctic and Antarctic sea ice: a synthesis. *Elem. Sci. Anthr.* **6**, 4 (2018).
93. Garrison, D. L. & Buck, K. R. The biota of Antarctic pack ice in the Weddell Sea and Antarctic Peninsula regions. *Polar Biol.* **10**, 211–219 (1989).
94. Arrigo, K. R. Sea ice ecosystems. *Annu. Rev. Mar. Sci.* **6**, 439–467 (2014).
95. Jeffery, N. et al. Investigating controls on sea ice algal production using E3SMv1.1-BGC. *Ann. Glaciol.* **61**, 51–72 (2020).
96. Kostov, Y. et al. Fast and slow responses of Southern Ocean sea surface temperature to SAM in coupled climate models. *Clim. Dyn.* **48**, 1595–1609 (2017).
97. Thompson, D. W. J. & Solomon, S. Interpretation of recent southern hemisphere climate change. *Science* **296**, 895–899 (2002).
98. Stuecker, M. F., Bitz, C. M. & Armour, K. C. Conditions leading to the unprecedented low Antarctic sea ice extent during the 2016 austral spring season. *Geophys. Res. Lett.* **44**, 9008–9019 (2017).
99. Ardyna, M. et al. Under-ice phytoplankton blooms: shedding light on the "invisible" part of Arctic primary production. *Front. Mar. Sci.* **7**, 608032 (2020).
100. Arrigo, K. R. et al. Massive phytoplankton blooms under Arctic Sea ice. *Science* **336**, 1408–1408 (2012).
101. Hague, M. & Vichi, M. Southern Ocean biogeochemical argo detect under-ice phytoplankton growth before sea ice retreat. *Biogeosciences* **18**, 25–38 (2021).
102. Balch, W. M. et al. Factors regulating the Great Calcite Belt in the Southern Ocean and its biogeochemical significance. *Glob. Biogeochem. Cycles* **30**, 1124–1144 (2016).
103. Holligan, P. M., Charalampopoulou, A. & Hutson, R. Seasonal distributions of the coccolithophore, *Emiliania huxleyi*, and of particulate inorganic carbon in surface waters of the Scotia Sea. *J. Mar. Syst.* **82**, 195–205 (2010).
104. Balch, W. M. Calcium carbonate measurements in the surface global ocean based on moderate-resolution imaging spectroradiometer data. *J. Geophys. Res.* **110**, C07001 (2005).
105. Chen, H., Haumann, F. A., Talley, L. D., Johnson, K. S. & Sarmiento, J. L. The deep ocean's carbon exhaust. *Glob. Biogeochem. Cycles* **36**, e2021GB007156 (2022).
106. Kaufman, D. E. et al. Climate change impacts on southern Ross Sea phytoplankton composition, productivity, and export. *J. Geophys. Res. Ocean.* **122**, 2339–2359 (2017).
107. Arrigo, K. R. et al. Phytoplankton community structure and the drawdown of nutrients and CO_2 in the Southern Ocean. *Science* **283**, 365–367 (1999).
108. Delmont, T. O., Hammar, K. M., Ducklow, H. W., Yager, P. L. & Post, A. F. *Phaeocystis antarctica* blooms strongly influence bacterial community structures in the Amundsen Sea polynya. *Front. Microbiol.* **5**, 646 (2014).
109. Oliver, H., St-Laurent, P., Sherrell, R. M. & Yager, P. L. Modeling iron and light controls on the summer *Phaeocystis antarctica* bloom in the Amundsen Sea polynya. *Glob. Biogeochem. Cycles* **33**, 570–596 (2019).
110. Yager, P. et al. A carbon budget for the Amundsen Sea polynya, Antarctica: estimating net community production and export in a highly productive polar ecosystem. *Elem. Sci. Anthr.* **4**, 000140 (2016).
111. Schine, C. M. S. et al. Massive Southern Ocean phytoplankton bloom fed by iron of possible hydrothermal origin. *Nat. Commun.* **12**, 1211 (2021).
112. Schoemann, V., Becquevort, S., Stefels, J., Rousseau, V. & Lancelot, C. *Phaeocystis* blooms in the global ocean and their controlling mechanisms: a review. *J. Sea Res.* **53**, 43–66 (2005).

113. Smith, H. E. K. et al. The influence of environmental variability on the biogeography of coccolithophores and diatoms in the Great Calcite Belt. *Biogeosciences* **14**, 4905–4925 (2017).
114. Vogt, M. et al. Global marine plankton functional type biomass distributions: *Phaeocystis* spp. *Earth Syst. Sci. Data* **4**, 107–120 (2012).
115. Arrigo, K. R. et al. Early spring phytoplankton dynamics in the western Antarctic Peninsula. *J. Geophys. Res. Ocean.* **122**, 9350–9369 (2017).
116. Biggs, T. E. G. et al. Antarctic phytoplankton community composition and size structure: importance of ice type and temperature as regulatory factors. *Polar Biol.* **42**, 1997–2015 (2019).
117. Kropuenske, L. R. et al. Photophysiology in two major Southern Ocean phytoplankton taxa: photoprotection in *Phaeocystis antarctica* and *Fragilariopsis cylindrus*. *Limnol. Oceanogr.* **54**, 1176–1196 (2009).
118. Trimborn, S. et al. Two Southern Ocean diatoms are more sensitive to ocean acidification and changes in irradiance than the prymnesiophyte *Phaeocystis antarctica*. *Physiol. Plant.* **160**, 155–170 (2017).
119. Fisher, B. J. et al. Biogeochemistry of climate driven shifts in Southern Ocean primary producers. *Biogeosciences Discuss.* https://doi.org/10.5194/bg-2023-10 (2023).
120. Lewis, K. M., van Dijken, G. L. & Arrigo, K. R. Changes in phytoplankton concentration now drive increased Arctic Ocean primary production. *Science* **369**, 198–202 (2020).
121. Stammerjohn, S., Massom, R., Rind, D. & Martinson, D. Regions of rapid sea ice change: an inter-hemispheric seasonal comparison. *Geophys. Res. Lett.* **39**, L06501 (2012).
122. Schine, C. M. S., Van Dijken, G. & Arrigo, K. R. Spatial analysis of trends in primary production and relationship with large-scale climate variability in the Ross Sea, Antarctica (1997–2013). *J. Geophys. Res. Ocean.* **121**, 368–386 (2016).
123. Del Castillo, C. E., Signorini, S. R., Karaköylü, E. M. & Rivero-Calle, S. Is the Southern Ocean getting greener? *Geophys. Res. Lett.* **46**, 6034–6040 (2019).
124. Thomalla, S. J., Fauchereau, N., Swart, S. & Monteiro, P. M. S. Regional scale characteristics of the seasonal cycle of chlorophyll in the Southern Ocean. *Biogeosciences* **8**, 2849–2866 (2011).
125. Eppley, R. W., Stewart, E., Abbott, M. R. & Heyman, U. Estimating ocean primary production from satellite chlorophyll. Introduction to regional differences and statistics for the Southern California Bight. *J. Plankton Res.* **7**, 57–70 (1985).
126. Monteiro, T., Kerr, R., Orselli, I. B. M. & Lencina-Avila, J. M. Towards an intensified summer CO_2 sink behaviour in the Southern Ocean coastal regions. *Prog. Oceanogr.* **183**, 102267 (2020).
127. Li, Y., Ji, R., Jenouvrier, S., Jin, M. & Stroeve, J. Synchronicity between ice retreat and phytoplankton bloom in circum-Antarctic polynyas. *Geophys. Res. Lett.* **43**, 2086–2093 (2016).
128. Liniger, G., Strutton, P. G., Lannuzel, D. & Moreau, S. Calving event led to changes in phytoplankton bloom phenology in the mertz polynya, Antarctica. *J. Geophys. Res. Ocean.* **125**, e2020JC016387 (2020).
129. Greaves, B. L. et al. The Southern Annular Mode (SAM) influences phytoplankton communities in the seasonal ice zone of the Southern Ocean. *Biogeosciences* **17**, 3815–3835 (2020).
130. Noh, K. M., Lim, H.-G. & Kug, J.-S. Zonally asymmetric phytoplankton response to the Southern annular mode in the marginal sea of the Southern Ocean. *Sci. Rep.* **11**, 10266 (2021).
131. Fu, W., Randerson, J. T. & Moore, J. K. Climate change impacts on net primary production (NPP) and export production (EP) regulated by increasing stratification and phytoplankton community structure in the CMIP5 models. *Biogeosciences* **13**, 5151–5170 (2016).
132. Leung, S., Cabré, A. & Marinov, I. A latitudinally banded phytoplankton response to 21st century climate change in the Southern Ocean across the CMIP5 model suite. *Biogeosciences* **12**, 5715–5734 (2015).
133. Kwiatkowski, L. et al. Twenty-first century ocean warming, acidification, deoxygenation, and upper-ocean nutrient and primary production decline from CMIP6 model projections. *Biogeosciences* **17**, 3439–3470 (2020).
134. Krishnamurthy, A. et al. Impacts of increasing anthropogenic soluble iron and nitrogen deposition on ocean biogeochemistry. *Glob. Biogeochem. Cycles* **23**, GB3016 (2009).
135. Sallée, J.-B. et al. Summertime increases in upper-ocean stratification and mixed-layer depth. *Nature* **591**, 592–598 (2021).
136. Moreau, S. et al. Climate change enhances primary production in the western Antarctic Peninsula. *Glob. Change Biol.* **21**, 2191–2205 (2015).
137. Schofield, O. et al. Changes in the upper ocean mixed layer and phytoplankton productivity along the west Antarctic Peninsula. *Phil. Trans. R. Soc. Math. Phys. Eng. Sci.* **376**, 20170173 (2018).
138. Hauck, J., Lenton, A., Langlais, C. & Matear, R. The fate of carbon and nutrients exported out of the Southern Ocean. *Glob. Biogeochem. Cycles* **32**, 1556–1573 (2018).
139. Moore, J. K. et al. Sustained climate warming drives declining marine biological productivity. *Science* **359**, 1139–1143 (2018).
140. Henson, S. A. et al. Uncertain response of ocean biological carbon export in a changing world. *Nat. Geosci.* **15**, 248–254 (2022).
141. Hauck, J. et al. Sparse observations induce large biases in estimates of the global ocean CO_2 sink: an ocean model subsampling experiment. *Phil. Trans. R. Soc. Math. Phys. Eng. Sci.* **381**, 20220063 (2023).
142. Moreau, S., Boyd, P. W. & Strutton, P. G. Remote assessment of the fate of phytoplankton in the Southern Ocean sea-ice zone. *Nat. Commun.* **11**, 3108 (2020).
143. Rohr, T., Richardson, A. J., Lenton, A., Chamberlain, M. A. & Shadwick, E. H. Zooplankton grazing is the largest source of uncertainty for marine carbon cycling in CMIP6 models. *Commun. Earth Env.* **4**, 212 (2023).
144. Yang, G., Atkinson, A., Pakhomov, E. A., Hill, S. L. & Racault, M. Massive circumpolar biomass of Southern Ocean zooplankton: implications for food web structure, carbon export, and marine spatial planning. *Limnol. Oceanogr.* **67**, 2516–2530 (2022).
145. Atkinson, A. et al. KRILLBASE: a circumpolar database of Antarctic krill and salp numerical densities, 1926–2016. *Earth Syst. Sci. Data* **9**, 193–210 (2017).
146. Trebilco, R., Baum, J. K., Salomon, A. K. & Dulvy, N. K. Ecosystem ecology: size-based constraints on the pyramids of life. *Trends Ecol. Evol.* **28**, 423–431 (2013).
147. Tittensor, D. P. et al. A protocol for the intercomparison of marine fishery and ecosystem models: fish-MIP v1.0. *Geosci. Model. Dev.* **11**, 1421–1442 (2018).
148. Dornan, T., Fielding, S., Saunders, R. A. & Genner, M. J. Large mesopelagic fish biomass in the Southern Ocean resolved by acoustic properties. *Proc. R. Soc. B* **289**, 20211781 (2022).
149. Hindell, M. A. et al. Tracking of marine predators to protect Southern Ocean ecosystems. *Nature* **580**, 87–92 (2020).
150. Chawarski, J., Klevjer, T. A., Coté, D. & Geoffroy, M. Evidence of temperature control on mesopelagic fish and zooplankton communities at high latitudes. *Front. Mar. Sci.* **9**, 917985 (2022).
151. Block, B. A. et al. Toward a national animal telemetry network for aquatic observations in the United States. *Anim. Biotelem.* **4**, 6 (2016).
152. Le Ster, L. et al. Improved accuracy and spatial resolution for bio-logging-derived chlorophyll a fluorescence measurements in the Southern Ocean. *Front. Mar. Sci.* **10**, 1122822 (2023).
153. Naito, Y. New steps in bio-logging science. *Mem. Natl. Inst. Polar Res.* **58**, 50–57 (2004).
154. Block, B. A. et al. Tracking apex marine predator movements in a dynamic ocean. *Nature* **475**, 86–90 (2011).
155. Labrousse, S. et al. Coastal polynyas: winter oases for subadult southern elephant seals in East Antarctica. *Sci. Rep.* **8**, 3183 (2018).
156. McMahon, C. R. et al. Animal borne ocean sensors — AniBOS — an essential component of the Global Ocean observing system. *Front. Mar. Sci.* **8**, 751840 (2021).
157. DuVivier, A. K. et al. Projections of winter polynyas and their biophysical impacts in the Ross Sea Antarctica. *Clim. Dyn.* **62**, 989–1012 (2023).
158. Hansell, D. A. & Carlson, C. A. (eds) *Biogeochemistry of Marine Dissolved Organic Matter* 2nd edn (Elsevier, 2015).
159. Eich, C. et al. Ecological importance of viral lysis as a loss factor of phytoplankton in the Amundsen Sea. *Microorganisms* **10**, 1967 (2022).
160. Hansell, D. A. & Orellana, M. V. Dissolved organic matter in the global ocean: a primer. *Gels* **7**, 128 (2021).
161. Bercovici, S. K. & Hansell, D. A. Dissolved organic carbon in the deep Southern Ocean: local versus distant controls: Southern Ocean DOC: local versus distant controls. *Glob. Biogeochem. Cycles* **30**, 350–360 (2016).
162. Boyd, P. W., Claustre, H., Levy, M., Siegel, D. A. & Weber, T. Multi-faceted particle pumps drive carbon sequestration in the ocean. *Nature* **568**, 327–335 (2019).
163. Lopez, C. N. & Hansell, D. A. Anomalous DOC signatures reveal iron control on export dynamics in the Pacific Southern Ocean. *Front. Mar. Sci.* **10**, 1070458 (2023).
164. Yu, J. et al. Sea ice melting drives substantial change in dissolved organic matter in surface water off Prydz Bay, East Antarctic. *J. Geophys. Res. Biogeosci.* **128**, e2023JG007415 (2023).
165. Genovese, C. et al. Influence of organic complexation on dissolved iron distribution in East Antarctic pack ice. *Mar. Chem.* **203**, 28–37 (2018).
166. Lannuzel, D., Grotti, M., Abelmoschi, M. L. & Van Der Merwe, P. Organic ligands control the concentrations of dissolved iron in Antarctic sea ice. *Mar. Chem.* **174**, 120–130 (2015).
167. Smith, A. J. R. et al. Identifying potential sources of iron-binding ligands in coastal Antarctic environments and the wider Southern Ocean. *Front. Mar. Sci.* **9**, 948772 (2022).
168. Norman, L. et al. The characteristics of dissolved organic matter (DOM) and chromophoric dissolved organic matter (CDOM) in Antarctic sea ice. *Deep. Sea Res. II* **58**, 1075–1091 (2011).
169. Biggs, T. E. G., Huisman, J. & Brussaard, C. P. D. Viral lysis modifies seasonal phytoplankton dynamics and carbon flow in the Southern Ocean. *ISME J.* **15**, 3615–3622 (2021).
170. Henson, S. A. et al. A seasonal transition in biological carbon pump efficiency in the northern Scotia Sea, Southern Ocean. *Deep. Sea Res. II* **208**, 105274 (2023).
171. Terrats, L. et al. BioGeoChemical-Argo floats reveal stark latitudinal gradient in the Southern Ocean deep carbon flux driven by phytoplankton community composition. *Glob. Biogeochem. Cycles* **37**, e2022GB007624 (2023).
172. Ratnarajah, L. et al. Distribution and export of particulate organic carbon in East Antarctic coastal polynyas. *Deep. Sea Res. I* **190**, 103899 (2022).
173. Omand, M. M. et al. Eddy-driven subduction exports particulate organic carbon from the spring bloom. *Science* **348**, 222–225 (2015).
174. Belcher, A. et al. Krill faecal pellets drive hidden pulses of particulate organic carbon in the marginal ice zone. *Nat. Commun.* **10**, 889 (2019).
175. Pinti, J., Jónasdóttir, S. H., Record, N. R. & Visser, A. W. The global contribution of seasonally migrating copepods to the biological carbon pump. *Limnol. Oceanogr.* https://doi.org/10.1002/lno.12335 (2023).
176. Takahashi, T. et al. Global sea–air CO_2 flux based on climatological surface ocean pCO_2, and seasonal biological and temperature effects. *Deep. Sea Res. II* **49**, 1601–1622 (2002).

177. Gruber, N. et al. The oceanic sink for anthropogenic CO_2 from 1994 to 2007. *Science* **363**, 1193–1199 (2019).
178. Huang, Y., Fassbender, A. J. & Bushinsky, S. M. Biogenic carbon pool production maintains the Southern Ocean carbon sink. *Proc. Natl Acad. Sci. USA* **120**, e2217909120 (2023).
179. Gregor, L., Kok, S. & Monteiro, P. M. S. Empirical methods for the estimation of Southern Ocean CO_2 support vector and random forest regression. *Biogeosciences* **14**, 5551–5569 (2017).
180. Le Quéré, C. & Saltzman, E. S. Introduction to surface ocean–lower atmosphere processes. In *Geophysical Monograph Series* Vol. 187 (eds Le Quéré, C. & Saltzman, E. S.) 1–5 (American Geophysical Union, 2009).
181. Pasquer, B., Metzl, N., Goosse, H. & Lancelot, C. What drives the seasonality of air–sea CO_2 fluxes in the ice-free zone of the Southern Ocean: a 1D coupled physical–biogeochemical model approach. *Mar. Chem.* **177**, 554–565 (2015).
182. Shadwick, E. H. et al. Sea ice suppression of CO_2 outgassing in the west Antarctic Peninsula: implications for the evolving Southern Ocean carbon sink. *Geophys. Res. Lett.* **48**, e2020GL091835 (2021).
183. Arrigo, K. R., Van Dijken, G. & Long, M. Coastal Southern Ocean: a strong anthropogenic CO_2 sink. *Geophys. Res. Lett.* **35**, L21602 (2008).
184. Keppler, L. & Landschützer, P. Regional wind variability modulates the Southern Ocean carbon sink. *Sci. Rep.* **9**, 7384 (2019).
185. Matear, R. J., Hirst, A. C. & McNeil, B. I. Changes in dissolved oxygen in the Southern Ocean with climate change. *Geochem. Geophys. Geosyst*. https://doi.org/10.1029/2000GC000086 (2000).
186. Sarmiento, J. L. & Le Quéré, C. Oceanic carbon dioxide uptake in a model of century-scale global warming. *Science* **274**, 1346–1350 (1996).
187. Uchida, T. et al. Vertical eddy iron fluxes support primary production in the open Southern Ocean. *Nat. Commun.* **11**, 1125 (2020).
188. Du Plessis, M. D. et al. The daily-resolved Southern Ocean mixed layer: regional contrasts assessed using glider observations. *J. Geophys. Res. Ocean.* **127**, e2021JC017760 (2022).
189. Boyd, P. W. et al. Mesoscale iron enrichment experiments 1993–2005: synthesis and future directions. *Science* **315**, 612–617 (2007).
190. Su, J., Schallenberg, C., Rohr, T., Strutton, P. G. & Phillips, H. E. New estimates of Southern Ocean annual net community production revealed by BGC-Argo floats. *Geophys. Res. Lett.* **49**, e2021GL097372 (2022).
191. Liniger, G., Moreau, S. Lannuzel, D. & Strutton P. Large contribution of the sea-ice zone to Southern Ocean carbon export revealed by BGC-Argo floats. Preprint at https://www.researchsquare.com/article/rs-3937570/v1 (2024).
192. Dinauer, A., Laufkötter, C., Doney, S. C. & Joos, F. What controls the large-scale efficiency of carbon transfer through the ocean's mesopelagic zone? Insights from a new, mechanistic model (MSPACMAM). *Glob. Biogeochem. Cycles* **36**, e2021GB007131 (2022).
193. Jaccard, S. L., Galbraith, E. D., Martínez-García, A. & Anderson, R. F. Covariation of deep Southern Ocean oxygenation and atmospheric CO_2 through the last ice age. *Nature* **530**, 207–210 (2016).
194. Ingrosso, G. et al. Physical and biological controls on anthropogenic CO_2 sink of the Ross Sea. *Front. Mar. Sci.* **9**, 954059 (2022).
195. Nissen, C., Timmermann, R., Hoppema, M., Gürses, Ö. & Hauck, J. Abruptly attenuated carbon sequestration with Weddell Sea dense waters by 2100. *Nat. Commun.* **13**, 3402 (2022).
196. Silvano, A. et al. Freshening by glacial meltwater enhances melting of ice shelves and reduces formation of Antarctic Bottom Water. *Sci. Adv.* **4**, eaap9467 (2018).
197. Rickard, G. J., Behrens, E., Bahamondes Dominguez, A. A. & Pinkerton, M. H. An assessment of the oceanic physical and biogeochemical components of CMIP5 and CMIP6 models for the Ross Sea region. *J. Geophys. Res. Ocean.* **128**, e2022JC018880 (2023).
198. Brown, M. S. et al. Enhanced oceanic CO_2 uptake along the rapidly changing west Antarctic Peninsula. *Nat. Clim. Change* **9**, 678–683 (2019).
199. Shadwick, E. H. et al. Glacier tongue calving reduced dense water formation and enhanced carbon uptake. *Geophys. Res. Lett.* **40**, 904–909 (2013).
200. Herraiz-Borreguero, L., Lannuzel, D., Van Der Merwe, P., Treverrow, A. & Pedro, J. B. Large flux of iron from the Amery Ice Shelf marine ice to Prydz Bay, East Antarctica. *J. Geophys. Res. Ocean.* **121**, 6009–6020 (2016).
201. Arroyo, M. C., Shadwick, E. H., Tilbrook, B., Rintoul, S. R. & Kusahara, K. A continental shelf pump for CO_2 on the Adélie land coast, East Antarctica. *J. Geophys. Res. Ocean.* **125**, e2020JC016302 (2020).
202. Krumhardt, K. M. et al. Potential predictability of net primary production in the Ocean. *Glob. Biogeochem. Cycles* **34**, e2020GB006531 (2020).
203. Freeman, N. M. & Lovenduski, N. S. Decreased calcification in the Southern Ocean over the satellite record. *Geophys. Res. Lett.* **42**, 1834–1840 (2015).
204. Volk, T. & Hoffert, M. I. Ocean carbon pumps: analysis of relative strengths and efficiencies in ocean-driven atmospheric CO_2 changes. In *The Carbon Cycle and Atmospheric CO_2: Natural Variations Archean to Present. Chapman Conference Papers, 1984*. Geophysical Monograph 32 (eds Sundquist, E. T. & Broecker, W. S.) 99–110 (American Geophysical Union, 1985).
205. Manno, C. et al. Threatened species drive the strength of the carbonate pump in the northern Scotia Sea. *Nat. Commun.* **9**, 4592 (2018).
206. Salter, I. et al. Carbonate counter pump stimulated by natural iron fertilization in the Polar Frontal Zone. *Nat. Geosci.* **7**, 885–889 (2014).
207. Rembauville, M. et al. Planktic foraminifer and coccolith contribution to carbonate export fluxes over the central Kerguelen Plateau. *Deep. Sea Res. I* **111**, 91–101 (2016).
208. Wynn-Edwards, C. A. et al. Particle fluxes at the Australian Southern Ocean Time Series (SOTS) achieve organic carbon sequestration at rates close to the global median, are dominated by biogenic carbonates, and show no temporal trends over 20-years. *Front. Earth Sci.* **8**, 329 (2020).
209. Neukermans, G. et al. Quantitative and mechanistic understanding of the open ocean carbonate pump — perspectives for remote sensing and autonomous in situ observation. *Earth Sci. Rev.* **239**, 104359 (2023).
210. Ryan-Keogh, T. J., Thomalla, S. J., Monteiro, P. M. S. & Tagliabue, A. Multidecadal trend of increasing iron stress in Southern Ocean phytoplankton. *Science* **379**, 834–840 (2023).
211. Henley, S. F. et al. Changing biogeochemistry of the Southern Ocean and its ecosystem implications. *Front. Mar. Sci.* **7**, 581 (2020).
212. Hutchins, D. A. & Boyd, P. W. Marine phytoplankton and the changing ocean iron cycle. *Nat. Clim. Change* **6**, 1072–1079 (2016).
213. van der Merwe, P., Trull, T. W., Goodwin, T., Jansen, P. & Bowie, A. The autonomous clean environmental (ACE) sampler: a trace-metal clean seawater sampler suitable for open-ocean time-series applications. *Limnol. Oceanogr. Meth.* **17**, 490–504 (2019).
214. Mitchell, G. B. & Holm-Hansen, O. Bio-optical properties of Antarctic Peninsula waters: differentiation from temperate ocean models. *Deep. Sea Res. I* **38**, 1009–1028 (1991).
215. Strzepek, R. F., Boyd, P. W. & Sunda, W. G. Photosynthetic adaptation to low iron, light, and temperature in Southern Ocean phytoplankton. *Proc. Natl Acad. Sci. USA* **116**, 4388–4393 (2019).
216. Andrew, S. M. et al. Widespread use of proton-pumping rhodopsin in Antarctic phytoplankton. *Proc. Natl Acad. Sci. USA* **120**, e2307638120 (2023).
217. Verdy, A. & Mazloff, M. R. A data assimilating model for estimating Southern Ocean biogeochemistry. *J. Geophys. Res. Ocean.* **122**, 6968–6988 (2017).
218. Gloege, L. et al. Quantifying errors in observationally based estimates of ocean carbon sink variability. *Glob. Biogeochem. Cycles* **35**, e2020GB006788 (2021).
219. Bushinsky, S. M. et al. Reassessing Southern Ocean air–sea CO_2 flux estimates with the addition of biogeochemical float observations. *Glob. Biogeochem. Cycles* **33**, 1370–1388 (2019).
220. Boyd, P. W. et al. Controls on polar Southern Ocean deep chlorophyll maxima: viewpoints from multiple observational platforms. *Glob. Biogeochem. Cycles* https://doi.org/10.1029/2023GB008033 (2023).
221. Mallet, M. D., Alexander, S. P., Protat, A. & Fiddes, S. L. Reducing Southern Ocean shortwave radiation errors in the ERA5 reanalysis with machine learning and 25 years of surface observations. *Artif. Intell. Earth Syst*. https://doi.org/10.1175/AIES-D-22-0044.1 (2023).
222. Rosso, I. et al. Water mass and biogeochemical variability in the kerguelen sector of the Southern Ocean: a machine learning approach for a mixing hot spot. *J. Geophys. Res. Ocean.* **125**, e2019JC015877 (2020).
223. Landschützer, P., Laruelle, G. G., Roobaert, A. & Regnier, P. A uniform pCO_2 climatology combining open and coastal oceans. *Earth Syst. Sci. Data* **12**, 2537–2553 (2020).
224. Kidston, M., Matear, R. & Baird, M. E. Phytoplankton growth in the Australian sector of the Southern Ocean, examined by optimising ecosystem model parameters. *J. Mar. Syst.* **128**, 123–137 (2013).
225. Schartau, M. et al. Reviews and syntheses: parameter identification in marine planktonic ecosystem modelling. *Biogeosciences* **14**, 1647–1701 (2017).
226. Kriest, I. et al. One size fits all? Calibrating an ocean biogeochemistry model for different circulations. *Biogeosciences* **17**, 3057–3082 (2020).
227. Melbourne-Thomas, J. et al. Optimal control and system limitation in a Southern Ocean ecosystem model. *Deep. Sea Res. II* **114**, 64–73 (2015).
228. Ward, B. A. et al. When is a biogeochemical model too complex? Objective model reduction and selection for North Atlantic time-series sites. *Prog. Oceanogr.* **116**, 49–65 (2013).
229. Losa, S. N., Kivman, G. A. & Ryabchenko, V. A. Weak constraint parameter estimation for a simple ocean ecosystem model: what can we learn about the model and data? *J. Mar. Syst.* **45**, https://doi.org/10.1016/j.jmarsys.2003.08.005 (2004).
230. Buitenhuis, E. T., Rivkin, R. B., Sailley, S. & Le Quéré, C. Biogeochemical fluxes through microzooplankton. *Glob. Biogeochem. Cycles* **24**, GB4015 (2010).
231. Buitenhuis, E. et al. Biogeochemical fluxes through mesozooplankton. *Glob. Biogeochem. Cycles* **20**, GB2003 (2006).
232. Le Quéré, C. et al. Role of zooplankton dynamics for Southern Ocean phytoplankton biomass and global biogeochemical cycles. *Biogeosciences* **13**, 4111–4133 (2016).
233. Strzepek, R. F. et al. Spinning the "ferrous wheel": the importance of the microbial community in an iron budget during the FeCycle experiment. *Glob. Biogeochem. Cycles* **19**, 2005GB002490 (2005).
234. Raiswell, R., Benning, L. G., Tranter, M. & Tulaczyk, S. Bioavailable iron in the Southern Ocean: the significance of the iceberg conveyor belt. *Geochem. Trans.* **9**, 7 (2008).
235. Laufkötter, C., Stern, A. A., John, J. G., Stock, C. A. & Dunne, J. P. Glacial iron sources stimulate the Southern Ocean carbon cycle. *Geophys. Res. Lett.* **45**, 13377–13385 (2018).
236. Ito, A., Ye, Y., Baldo, C. & Shi, Z. Ocean fertilization by pyrogenic aerosol iron. *npj Clim. Atmos. Sci.* **4**, 30 (2021).
237. Bowie, A. R. et al. The fate of added iron during a mesoscale fertilisation experiment in the Southern Ocean. *Deep. Sea Res. II* **48**, 2703–2743 (2001).
238. Law, C. S., Abraham, E. R., Watson, A. J. & Liddicoat, M. I. Vertical eddy diffusion and nutrient supply to the surface mixed layer of the Antarctic Circumpolar Current. *J. Geophys. Res. Ocean.* **108**, 2002JC001604 (2003).

239. Blain, S. et al. Effect of natural iron fertilization on carbon sequestration in the Southern Ocean. *Nature* **446**, 1070–1074 (2007).
240. Watson, A. J. et al. Minimal effect of iron fertilization on sea-surface carbon dioxide concentrations. *Nature* **371**, 143–145 (1994).
241. De Jong, J. et al. Natural iron fertilization of the Atlantic sector of the Southern Ocean by continental shelf sources of the Antarctic Peninsula: iron fertilization from Antarctic continental shelf. *J. Geophys. Res. Biogeosci.* **117**, G01029 (2012).
242. Tagliabue, A. et al. Constraining the contribution of hydrothermal iron to Southern Ocean export production using deep ocean iron observations. *Front. Mar. Sci.* **9**, 754517 (2022).
243. Wu, S.-Y. & Hou, S. Impact of icebergs on net primary productivity in the Southern Ocean. *Cryosphere* **11**, 707–722 (2017).
244. Büchner, M. *ISIMIP3b ocean input data (v1.4)* (ISIMIP Repository); https://data.isimip.org/10.48364/ISIMIP.575744.4.
245. MacCready, P. & Quay, P. Biological export flux in the Southern Ocean estimated from a climatological nitrate budget. *Deep. Sea Res. II* **48**, 4299–4322 (2001).
246. Louanchi, F. & Najjar, R. G. Annual cycles of nutrients and oxygen in the upper layers of the North Atlantic Ocean. *Deep. Sea Res. II* **48**, 2155–2171 (2001).

Acknowledgements

The authors acknowledge the Fisheries and Marine Ecosystem Model Intercomparison Project coordinators and modellers for providing the model projections used in Fig. 4 and in Supplementary Figs. 1–4 of this paper. C.N. and D.L. were supported by the Australian Research Council (ARC) FT210100798 and FT190100688 respectively. P.W.B. was funded by an ARC Laureate (FL160100131). A.M.K. acknowledges funding from SOCCOM (OPP-1936222). S.J.T. was supported through the CSIR's Southern Ocean Carbon — Climate Observatory (SOCCO) Programme (http://socco.org.za/) funded by the Department of Science and Innovation (DSI/CON C3184/2023), the CSIR's Parliamentary Grant (0000005278) and the National Research Foundation (MCR210429598142). G.N. has received funding from the European Research Council (ERC) under the European Union's Horizon 2020 research and innovation programme (grant 853516 CarbOcean). S.S. was funded by a Wallenberg Academy Fellowship (WAF 2015.0186) and the Swedish Research Council (VR 2019–04400) and supported by the European Unions Horizon 2020 research and innovation programme under grant 821001 (SO-CHIC). E.H.S., P.W.B. and D.L. received grant funding from the Australian Government as part of the Antarctic Science Collaboration Initiative programme. This research was also supported by the Australian Research Council Special Research Initiative, Australian Centre for Excellence in Antarctic Science (project number SR200100008).

Author contributions

All authors researched data for the article. P.W.B., K.R.A., M.A., A.M.K., L.H., D.L., G.N., C.N., E.H.S., S.S. and S.J.T. contributed substantially to discussion of the content. P.W.B., K.R.A., D.L., G.N., C.N., E.H.S. and S.S. wrote the article. P.W.B., K.R.A., M.A., A.M.K., L.H., D.L., G.N., E.H.S., S.S. and S.J.T. reviewed and/or edited the manuscript before submission.

Competing interests

The authors declare no competing interests.

Additional information

Supplementary information The online version contains supplementary material available at https://doi.org/10.1038/s43017-024-00531-3.

Peer review information *Nature Reviews Earth & Environment* thanks Channing Prend, Lydia Keppler, Cara Nissen and the other, anonymous, reviewer for their contribution to the peer review of this work.

Related links

BGC-Argo: https://biogeochemical-argo.org/index.php
B-SOSE: https://soccom.princeton.edu/content/biogeochemical-sose-solution-now-available
Coupled Model Intercomparison Project: https://www.wcrp-climate.org/wgcm-cmip
FishMIP: www.fishmip.org
KRILLBASE: https://www.bas.ac.uk/project/krillbase/
NASA PACE: https://pace.oceansciences.org/home.htm
National Snow and Ice Data Centre: https://nsidc.org/arcticseaicenews/2023/09/antarctic-sets-a-record-low-maximum-by-wide-margin/
OC-CCI: https://www.oceancolour.org/
SOCLIM: http://soclim.com/

[1]Australian Centre for Excellence in Antarctic Science, University of Tasmania, Hobart, Tasmania, Australia. [2]Australian Antarctic Program Partnership, Institute for Marine and Antarctic Studies, University of Tasmania, Hobart, Tasmania, Australia. [3]Institute for Marine and Antarctic Studies, University of Tasmania, Hobart, Tasmania, Australia. [4]Department of Earth System Science, Stanford University, Stanford, CA, USA. [5]Takuvik Joint International Laboratory, Laval University (Canada) — CNRS (France), Département de biologie et Québec-Océan, Université Laval, Québec, QC, Canada. [6]National Institute of Water and Atmospheric Research, Hataitai, Wellington, New Zealand. [7]Centre for Ecology and Conservation, College of Life & Environmental Sciences, University of Exeter, Penryn Campus, Cornwall, United Kingdom. [8]Scripps Institution of Oceanography, UC San Diego, La Jolla, CA, USA. [9]Ghent University, Biology Department, MarSens Research Group, Ghent, Belgium. [10]Flanders Marine Institute (VLIZ), Ostend, Belgium. [11]CSIRO Environment, Hobart, Tasmania, Australia. [12]Department of Marine Sciences, University of Gothenburg, Gothenburg, Sweden. [13]Department of Oceanography, University of Cape Town, Rondebosch, South Africa. [14]Southern Ocean Carbon — Climate Observatory, CSIR, Cape Town, South Africa. [15]Marine and Antarctic Research Centre for Innovation and Sustainability, University of Cape Town, Cape Town, South Africa.